OCEAN SWELL DECAY OBSERVED OVER RELATIVELY SHORT DISTANCES WITH DIRECTIONAL BUOYS

Júlia Kaiser Sant' Anna

Rio de Janeiro
Setembro de 2020

OCEAN SWELL DECAY OBSERVED OVER RELATIVELY SHORT
DISTANCES WITH DIRECTIONAL BUOYS

Júlia Kaiser Sant' Anna

DISSERTAÇÃO SUBMETIDA AO CORPO DOCENTE DO INSTITUTO
ALBERTO LUIZ COIMBRA DE PÓS-GRADUAÇÃO E PESQUISA DE
ENGENHARIA DA UNIVERSIDADE FEDERAL DO RIO DE JANEIRO COMO
PARTE DOS REQUISITOS NECESSÁRIOS PARA A OBTENÇÃO DO GRAU
DE MESTRE EM CIÊNCIAS EM ENGENHARIA OCEÂNICA.

Orientadores: Nelson Violante de Carvalho
Uggo Ferreira de Pinho

Aprovada por: Prof. Nelson Violante de Carvalho
Prof. Luigi Cavaleri
Prof. Jesus Portilla Yandun
Prof. Carlos Eduardo Parente Ribeiro
Prof. Leandro Farina
Prof. Luiz Mariano Paes de Carvalho Filho

RIO DE JANEIRO, RJ – BRASIL
SETEMBRO DE 2020

It ain't what you don't know that gets you into trouble. It's what you know for sure that just ain't so.

Mark Twain

Acknowledgements

First of all, I would like to thank my parents, Tania and João, for supporting me throughout my entire life, including this long academic journey.

I am grateful to my advisor, Nelson, who trusted in my potential to develop this work many times more than myself.

Many thanks to my life partner Leonardo, who is increasingly dedicated to learning about the incredible waves to which I dedicate my professional and academic life.

Special thanks to my great tutor in life, Izabel Nogueira, who never hesitated to help and instruct me during all these years that I am working with her.

I thank Professor Carlos Eduardo Parente, who inspires me every day without even knowing it. Parente, all your knowledge and your pleasure in teaching are incredible and always motivates me.

I would like to thank all my colleagues from LIOc for making the job easier and more enjoyable.

I also thank the friends I made during the master's classes, Alex, Pedro Coelho and Lucas. You guys are amazing and made this period a lot more fun and peaceful.

DECAIMENTO DE SWELL EM DISTÂNCIAS RELATIVAMENTE CURTAS UTILIZANDO BOIAS DIRECIONAIS

Júlia Kaiser Sant' Anna

Setembro/2020

Orientadores: Nelson Violante de Carvalho
Uggo Ferreira de Pinho

Programa: Engenharia Oceânica

Swells são ondas capazes de viajar por longas distâncias sem uma perda de energia significativa. O decaimento de swell nos oceanos ainda não é completamente compreendido e a maioria dos trabalhos recentes sobre o tema utiliza dados de satélite e impõe um limite de distância mínimo para calcular o decaimento. Aqui, eventos de chegada dispersiva registrados por duas boias direcionais fundeadas em águas profundas na região sudoeste do Atlântico Sul – relativamente próximas da área de geração dos swells –, distantes cerca de 915 km uma da outra, são analisados. Técnicas de particionamento espectral são utilizadas para isolar as componentes de swell. A posição e as demais características da tempestade são obtidas com base nas informações dos campos de vorticidade relativa em 850 hPa. A taxa de variação de energia é calculada utilizando duas formulações presentes na literatura. Além disso, um método que leva em consideração as características da tempestade é proposto. A comparação dos resultados obtidos mostra que o modelo que depende da frequência e da distância melhor se adequa aos dados analisados. O método proposto produz resultados equivalentes àqueles obtidos utilizando o método dependente da frequência e da distância para o evento cuja distância de referência é de cerca de 2400 km. A taxa de decaimento média encontrado é de $1.4 \times 10^{-6} m^{-1}$, considerando distâncias de referência inferiores a 2500 km. Este resultado é uma ordem de grandeza superior aos reportados na literatura considerando distâncias de referência maiores. Assim, a taxa de decaimento de swells é maior em regiões mais próximas da área de geração. Além disso, os resultados encontrados mostram que o decaimento do swell não depende somente da distância mas também da frequência das ondas, de modo que as características da tempestade também têm importância neste processo.

Abstract of Dissertation presented to COPPE/UFRJ as a partial fulfillment of the requirements for the degree of Master of Science (M.Sc.)

OCEAN SWELL DECAY OBSERVED OVER RELATIVELY SHORT DISTANCES WITH DIRECTIONAL BUOYS

Júlia Kaiser Sant' Anna

September/2020

Advisors: Nelson Violante de Carvalho
          Uggo Ferreira de Pinho

Department: Ocean Engineering

Swells can propagate over large distances without significant energy loss. Despite several recently published papers about this subject, swell decay in the ocean is not yet completely understood. Most published works employed satellite data and imposed a threshold distance to compute the decay. Here, we analyse events of dispersive arrivals recorded by two directional buoys moored in deep water 915 km apart from each other in the southwest South Atlantic. The buoys are relatively closer to the storm's position, in respect with the recently published results that impose a distance in general superior to three thousand kilometers. Spectral partitioning techniques are employed to isolate the swell components. Hence, the storm's position is computed and also the storm features based on the characteristics of the vorticity field at 850 hPa level. The rate of energy variation is calculated using two distinct approaches presented in the literature for swell decay, one distance-only and the other distance-frequency dependent. In addition, a method for swell decay based on the storm features is proposed. The inter-evaluation of the results shows that the distance-frequency dependent method best fits our data. The storm features based method produced equivalent results to those obtained using distance-frequency dependent relation for the event whose reference distance is about 2400 km. The average swell decay rate is $1.4 \times 10^{-6} m^{-1}$, within reference distances inferior to 2500 km. That is one order of magnitude larger than the rate reported in the literature, for greater reference distances. Therefore, the decay rate is stronger for the waves closer to their generating storms. Furthermore, it is clear that the decay is not only dependent on distance, but wave frequency as well. The storm features may also play a role.

Contents

List of Figures

List of Tables

Chapter 1

Introduction

Swells can propagate over thousands of kilometers with little attenuation, therefore with low energy dissipation. SNODGRASS *et al.* (1966) presented a pioneering investigation that estimated the rate of swell dissipation based on *in-situ* measurements from an array of sensors deployed along a great circle in the Pacific Ocean. However, despite the importance for scientific, operational and recreational issues, swell evolution is not completely understood, mainly because of the complexity to track them over large distances with enough accuracy. This topic has received renewed attention, boosted by the broad coverage attained with sensors on-board satellites (ARDHUIN *et al.*, 2009; COLLARD *et al.*, 2009; JIANG *et al.*, 2016; YOUNG *et al.*, 2013).

Synthetic Aperture Radar (SAR) is so far the only spaceborne instrument that can yield the 2D directional spectrum, despite some limitations in the high frequency band caused by the orbital motions, the so-called azimuthal cut-off (HASSELMANN *et al.*, 2012). Furthermore, the retrieval of wave spectra from SAR images is a cumbersome operation, prone to inaccuracies (PORTILLA-YANDÚN *et al.*, 2019). The first wave scatterometer on-board a satellite, also capable to measure the directional spectrum, has been recently launched and is expected to overcome the limitations inherent to SAR measurements (HAUSER *et al.*, 2017). Significant wave height (SWH), on the other hand, measured from a myriad of altimeters with high accuracy, is available on several well-calibrated databases over the time span of around three decades — such as RIBAL and YOUNG (2019). However, SWH is a single spectral parameter that requires collocation with additional information when employed to analyse swell evolution.

ARDHUIN *et al.* (2009) — using a technique described in COLLARD *et al.* (2009) — employed 4 years of SAR Wave Mode data to analyse swell propagation and decay using 22 carefully selected events. The case selection procedure considered wind speed less than 9 m/s, swell heights larger than 0.5 m and also ignored data within 4000 km of the originating storm. COLLARD *et al.* (2009) demonstrated that

swell energy should be within 20% of the asymptotic values for distances αR larger than 4000 km from the storm location (α is spherical distance and R is the Earth radius). Semi-analytic functions were fitted using three models: a linear model, in which the decay rate μ depends on distance only; and two non-linear models that are dependent on the frequency and on the significant orbital velocity. Their estimated linear decay rate was of the same order as reported by SNODGRASS *et al.* (1966) — i.e. $10^{-7} m^{-1}$.

BABANIN and HAUS (2009) reported a decay rate of monochromatic waves generated in a wave tank proportional to a^3, where a is the wave amplitude. The formulation for swell decay proposed by BABANIN (2011) and BABANIN (2012) using the same experimental data assumed a mechanism similar to the one proposed by ARDHUIN *et al.* (2009), but with distinct theoretical suppositions. ARDHUIN *et al.* (2009) related swell decay to atmospheric turbulence whereas BABANIN (2011) and BABANIN (2012) considered turbulence on the water side. So, based on experimental results, BABANIN (2012) found attenuation rates 2.5 times on average larger than those obtained using the linear model presented by ARDHUIN *et al.* (2009).

YOUNG *et al.* (2013) combined SWH altimeter data with spectral information from a wave model reanalysis database. Descending passes coincident with great circle paths covering 24 years were selected to track down swells in the Southern Ocean. They considered specific propagation directions obtained from wave models and with low altimeter wind speeds. A total of 212 cases were assumed as unimodal systems to ensure that the altimeter SWH was in fact related to a single spectral partition. Distance from the generation area was less restrictive, imposing 1400 km as a threshold. Their results for swell decay are similar to the functional forms proposed by both ARDHUIN *et al.* (2009) and BABANIN (2012), but, according to JIANG *et al.* (2016), YOUNG *et al.* (2013) did not consider the attenuation associated with spherical spreading and therefore their swell decay rate is an order of magnitude higher.

JIANG *et al.* (2016), in a similar approach, used nearly 10 years of global altimeter measurements to track 202 swells events. SWH altimeter data were combined with wave direction and peak period from a collocated wave model, assuming as well unimodal or quasi-unimodal systems, in the sense that the totality of the altimeter SWH energy was related to a single swell partition. Only the measurements more than 4000 km from the generation area were retained for the analysis. The methods and results obtained are similar to those presented by ARDHUIN *et al.* (2009).

Therefore, the use of satellite data to investigate swell evolution has limitations, despite their high spatial and temporal coverage and large databases spanning many years. The retrieval of wave spectra from SAR images is a cumbersome procedure, specially for azimuth propagating waves. Additionally, the retrieval of waves pro-

pagating in any direction but with low energy is less accurate — those cases were excluded in ARDHUIN *et al.* (2009). Overall, SWH from SAR data is less accurate than those estimated from altimeters, although the content of wave energy over frequency is discernible, at least for low wavenumber, long swell waves. To get the distribution of SWH from altimeters over spectral partitions, when necessary, is a procedure liable to error and hence avoided in JIANG *et al.* (2016) and YOUNG *et al.* (2013). However, the selection of assumed unimodal cases can mislead the analysis of the transformation of directional wave energy over large distances.

Here, two directional buoys spaced 915 km apart in the Southwestern Atlantic are employed to investigate swell propagation and decay in comparatively short distances — as compared with the mentioned previous works. With the exception of the study carried out by SNODGRASS *et al.* (1966), which used *in-situ* measurements as well, all previous works analysed swell energy attenuation in the far field, with a stipulated minimum distance from the generating area. In the case of BABANIN (2012), experimental data from a wave tank were used. In the present paper, measurements significantly closer to the generating storm were retained. Spectral partitioning techniques are employed on the typically observed multi-modal wave spectra to track down swell propagating along the great circle formed by the buoys. Our main purpose is to investigate swell attenuation between two directional buoys during selected events. In all events, the downwave buoy is located less than 2500 km away from the generation storms. The linear formulation, the nonlinear formulation (BABANIN, 2012) and a here proposed storm feature dependent approach for swell decay are evaluated using our data.

The remainder is organized as follows. Chapter 2 addresses the data used and the methodology involved in analyzing swell data. In chapter 3 the results for swell decay are presented and discussed. Conclusions follow in chapter 4.

Chapter 2

Methodology

2.1 Study area and directional buoys dataset

Two Axys-3M directional buoys both at a depth of around 200 m off the South-Southeast Brazilian coast (PEREIRA *et al.*, 2017) are employed in the analysis. The southernmost (RG, see Figure 2.1) is 915 km away from the northernmost one (SA), in a SW-NE orientation. Also shown in Figure 2.1 is the great circle (yellow dotted line) passing between them, which is coincident with the main swell propagation direction in the region (PIANCA *et al.*, 2010; VIOLANTE-CARVALHO *et al.*, 2004). Because of operational issues, only about 16 months of simultaneously available directional data are used — five months in 2012 and eleven months in 2014-2015. Every hour, the buoys record heave-pitch-roll for 17 minutes with a sampling rate of 1.28 Hz. More details about the buoys configuration and estimation of parameters in PEREIRA *et al.* (2017). The directional wave spectra were obtained using FFT with a Hanning window, 50% of overlap and 16 degrees of freedom. The wave spectra have directional resolution of $6°$ (linearly spaced) and a logarithmically spaced frequency vector with 61 bins, ranging from 0.0418 Hz to 0.2461 Hz. Here, the factor 1.03 for the geometric progression was chosen in order to better distinguish the correct frequency of each swell system.
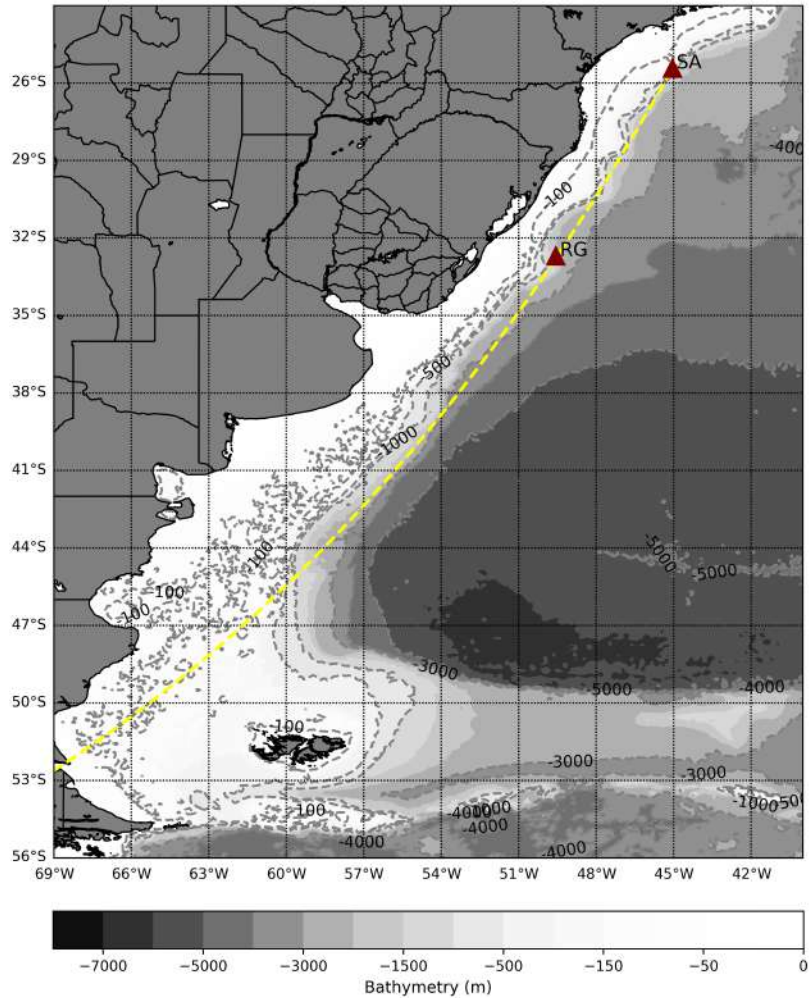
Figure 2.1: Study Area, the South-Southeast coast of Brazil, in the South Atlantic. The dotted yellow line is the great circle passing between the directional buoys (red triangles) moored off the coast of Rio Grande (RG) and Santos (SA) cities.

2.2 Spectral partitioning

A spectral partitioning technique allows the identification and separation of different wave systems that compose a spectrum. All partitions are described by a reduced set of parameters, such as wave height, period and direction, as well as their individual — separated — directional spectra $S(f, \theta)$, with θ as wave direction and f as frequency. Based on the approach presented in GERLING (1992), HASSELMANN *et al.* (1996) used the method to compare wave spectra retrieved from ERS-1 SAR Wave Mode data against the WAM wave model. VIOLANTE-CARVALHO

et al. (2005) made some modifications to HASSELMANN *et al.* (1996)'s method to tune it up for the particularities of the South Atlantic, characterized by multi-modal wave spectra with most of the spectral energy contained in the low frequency band. This is the spectral partitioning technique used in the present work.

2.3   Event selection criteria

For waves generated in a same storm, their frequency and direction measured in the buoys are expected to vary slowly, as a result of wave dispersion and storm evolution. Therefore, a given partitioned pair — frequency-direction — is sought in a previous measurement, recursively, over the duration of a selected dispersive arrival. The propagation direction is naturally restricted to the great circle passing between the two buoys, with azimuth $207.5° \pm 30°$ (Figure 2.1). Moreover, as lower frequency waves propagate faster than the longer frequency waves, frequency increases of at most 0.02 Hz per hour are included in the selection procedure, although some slight decrease of less than 0.0045 Hz are also acceptable because of instrumental accuracy and resolution.

2.4   Swell source area

According to the Linear Theory, the dispersion relation in deep water reads

$$f^2 = \frac{gk}{(2\pi)^2},\tag{2.1}$$

where f is linear frequency, k is wavenumber and g is the gravitational acceleration, hence waves are dispersive in frequency. It is possible to rewrite equation 2.1 in terms of group velocity C_g, distance d and time t.

$$C_g = \frac{g}{(4\pi)f} = \frac{d}{(t - t_0)}.\tag{2.2}$$

where $t - t_0$ is the time interval taken by the wave group to travel the distance d.

Based on the dispersive arrival, the distance traveled by the wave group is readily obtained.

$$d = \frac{g}{4\pi \frac{df}{dt}}.$$

(2.3)

Using concepts of spherical geometry, the coordinates of the storm generating area is given by (HANSON and PHILLIPS, 2001)

$$\Phi = sin^{-1}(sin\Phi_0 cos\theta_d + cos\Phi_0 sin\theta_d cos\bar{\theta})$$
$$\phi = \phi_0 - sin^{-1}\left(\frac{sin\theta_d sin\bar{\theta})}{cos\Phi}\right),$$

(2.4)

where Φ is latitude and ϕ is longitude of the (punctual) swell source area, Φ_0 and ϕ_0 are the latitude and longitude of the measurement, respectively; and θ_d is the angular distance. The coordinates of the computed generating storm area were compared with the wind and surface pressure fields of the Climate Forecast System Reanalysis (CFSR) from the National Centers for Environmental Prediction (NCEP). CFSR was also employed to estimate size and propagation speed of the storms (see details about the model configuration in SAHA *et al.*, 2010) — and some validation exercises in CAMPOS and SOARES (2017); SHARP *et al.* (2015); LINDSAY *et al.* (2014).

2.5   Swell decay rate

ARDHUIN *et al.* (2009) using SAR Wave Mode data presented a methodology to compute swell attenuation and dissipation rates, proposing the following linear model for the attenuation rate μ_a

$$\mu_a = \frac{-1}{R(\alpha_i - \alpha_0)} ln\left(\frac{E_s(\alpha_i)}{E_s(\alpha_0)}\right)$$

(2.5)

where R is the Earth radius and α is the distance in radians — α_0 is a reference distance — and E_s is the swell energy. Furthermore, a linear model for the dissipation rate μ is also presented (ARDHUIN *et al.*, 2009), also function of distance only:

$$\mu = \frac{-1}{R(\alpha_i - \alpha_0)} ln \left(\frac{E_s(\alpha_i)\alpha_i sin(\alpha_i)}{E_s(\alpha_0)\alpha_0 sin(\alpha_0)} \right) \tag{2.6}$$

ARDHUIN *et al.* (2009) and BABANIN (2012) also proposed nonlinear models for estimation of swell decay. Both models take into account wave period and have a dissipation factor to fit their data, but their formulations are, however, theoretically distincts. ARDHUIN *et al.* (2009)'s formulation is based on the wave coupling with the turbulent atmospheric boundary layer. The one proposed by BABANIN (2012), on the other hand, is based on the mechanism of turbulent flow on the water side.

The decay rate proposed in BABANIN (2012) is proportional to wavenumber k and amplitude a, reading

$$\frac{da^2(x)}{dx} = -\frac{4}{3}b1k^2a^3 \tag{2.7}$$

where x is the distance from the storm center in meters and $b1$ is a swell attenuation coefficient. In terms of swell significant wave height (H_{ss}), the swell decay based on BABANIN (2012)'s formulation μ_B can be obtained as

$$\mu_B = \frac{1 + \frac{1}{3}b1(Hss_0k^2x)}{x} \tag{2.8}$$

where H_{ss_0} is the swell height in a reference point.

Despite the fact that the storms responsible for generating the swell systems were less than 4000 km away from the southernmost buoy (minimum distance analyzed in ARDHUIN *et al.* (2009) and JIANG *et al.* (2016) works), the results will be

compared against the linear model proposed in ARDHUIN *et al.* (2009) and the nonlinear model by BABANIN (2012). The swell factor f_e proposed in ARDHUIN *et al.* (2009) can be estimated from $b1$ values (BABANIN, 2012)

$$b1 = 24f_e\frac{\rho_a}{\rho_w} \tag{2.9}$$

where ρ_a and ρ_w are the density of air and water, respectively. The f_e values computed using equation 2.9 will be used as reference.

2.5.1 Dependence of swell decay on the storm's features

The intensity, size and average speed of extratropical cyclones are closely related to the features of the waves generated by them. Despite their importance, the determination of these properties is challenging owing to the non-existence of a sole consensual methodology and, consequently, with discrepancies between reported comparisons (NEU *et al.*, 2013). Particularly challenging is the determination of its size, since a vortex has no clear delimitation from the flow field itself and arbitrary selection conditions are generally imposed. Here, we mainly follow the procedure described in FLAOUNAS *et al.* (2014), applying the methodology to the wind field estimated from the CFSR at 850 hPa level. As already mentioned, CFSR is the reanalysis model from NCEP and has spatial resolution of about 38 km (T382) with 64 vertical levels. In addition to the wind field at 10 m, here the wind fields at 850 hPa and the pressure field reduced to mean sea level both projected on a regular grid with spatial resolution of 0.50° are used.

The procedure for cyclone identification and characterization initially computes the smoothed relative vorticity field at 850 hPa level applying a spatial filter to remove noisy field gradients, in the form

$$M_{vor} = \frac{1}{(2X+1)^2} \cdot \sum_{i=a-X}^{a+X} \sum_{j=b-X}^{b+X} \left(M_{vor_{i,j}}\right) \tag{2.10}$$

where X by X is the pixel window, M_{vor} is the relative vorticity matrix and (a, b)

are the grid points. Imposing $X = 4$ means an area of approximately 500 km by 500 km, roughly the length scale of the expected cyclones. A threshold value of $-0.5 \times 10^{-5} s^{-1}$ (optimized after manual inspection) was applied to suppress small vorticity features and enhance the more relevant ones. The closest maximum vorticity field indicated by the dispersive arrival method is considered as the storm area and the storm position is subsequently determined every two hours over a period of 12 hours, 8 hours preceding and 4 hours following the time t_0 indicated by the dispersive arrival fit using the Linear Theory. It is then employed to determine the cyclone average speed (computed from the distance of the centers for consecutive time steps) and average properties.

The local maximum of the vorticity field determines its geographical coordinate and naturally its maximum vorticity at 850 hPa, alongside with the maximum wind speed at the level of 850 hPa. The cyclone radius is estimated considering a circle centered in the geographical coordinate imposing that the average vorticity within its radius is $1/3$ of the maximum vorticity. Several properties are quantified, such as the maximum and mean wind speed at 850 hPa (m/s), maximum and mean vorticity at 850 hPa ($1/s$), geographical position and the average propagation speed of the cyclone (V, in m/s). Hence, seeking for relationships between the rate of swell attenuation within relatively short distances from the storm area and the storm features (SF), the follow adimensional formulation is proposed for the swell attenuation coefficient $b1$, used in equation 2.11

$$b1_{SF} = \frac{V x}{df D^2} \qquad (2.11)$$

where V is the estimated propagation speed of the extratropical cyclone (m/s), df is the spectral bandwidth (Hz) of the wave records — calculated in terms of the 3 dB point (half-power) — D is the estimated storm diameter (m) and x is the distance (m) from the downwave buoy to the storm's center. Therefore, Hss in a specific

point can be computed as

$$Hss = \frac{Hss_0}{1 + (b1_{SF} Hss_0 k^2 x)} \tag{2.12}$$

2.5.2 Selection of Hss pairs

The cross-assignment of spectral parameters measured by both buoys is critical to compute the attenuation and dissipation rates. The selection was performed assuming the following criteria:

- Three-point moving average for the parameters time series of the spectral partitions: significant wave height of the swell partition (Hss), and correspondent frequency and direction for both buoys;

- Cross-assign the RG buoy points in frequency to their SA buoy counterpart;

- For a given selected frequency in the previous item, choose the closest in time to reach the northernmost buoy following the propagation time given by the Linear Theory.

The output of the procedure are correlated Hss, frequency and direction for each moment during the dispersive arrival event, according to the dispersion in frequency experienced by the waves between the buoys. Therefore, swell decay rate can be finally computed.

Chapter 3

Results and Discussions

3.1   Dispersive arrival and storm's position

Five events of dispersive arrival were selected out of the 16 months considered —
more details about the characteristics of all events are listed in appendix A. Figure
3.1 shows one of the selected cases of spectral evolution in buoy RG (top panel)
and buoy SA buoy (bottom panel) during a dispersive arrival. The swell system is
concentrated in a narrow spectral band with the gradual energy migration towards
higher frequencies clearly discernible — highlighted in Figure 3.1. The extracted
parameters of this event are also presented in Figure 3.2 (buoy RG) and Figure 3.3
(buoy SA). The features of a dispersive arrival are depicted by the time evolution of
swell frequency towards higher frequencies, clearly observed in both buoys — upper
panels. Also evident is the energy evolution described as H_{ss}, increasing up to the
storm peak energy followed by a decrease — middle panels. It is observed as well the
decrease of energy from buoy RG to buoy SA, as the waves propagate northwards.
The direction associated with the peak frequency is relatively constant, as shown in
the bottom panels.
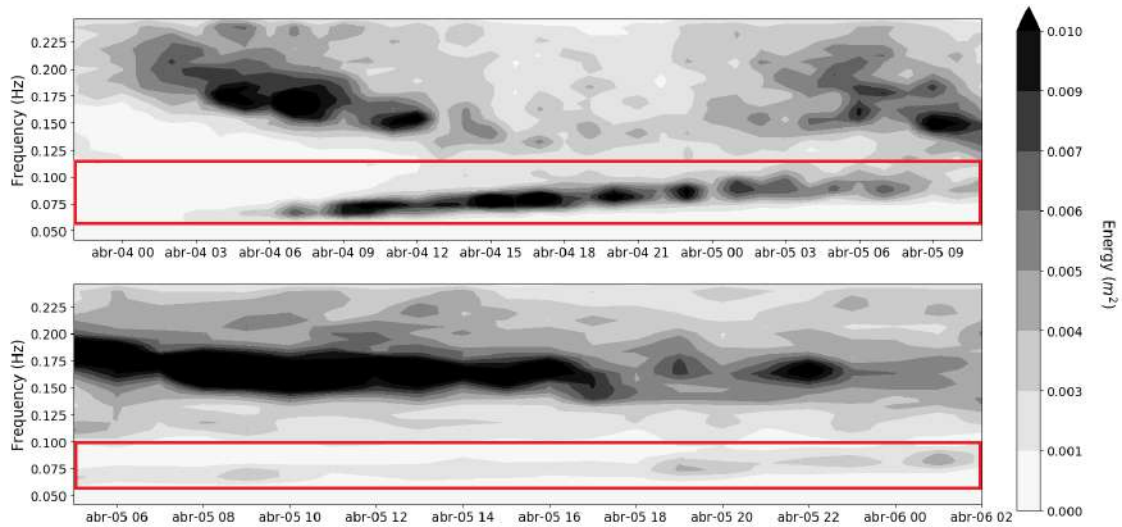
Figure 3.1: Evolution of the spectral energy over time during the dispersive arrival event recorded by buoy RG (top panel) and buoy SA (bottom panel) in April 2015. The red box highlights the selected event.
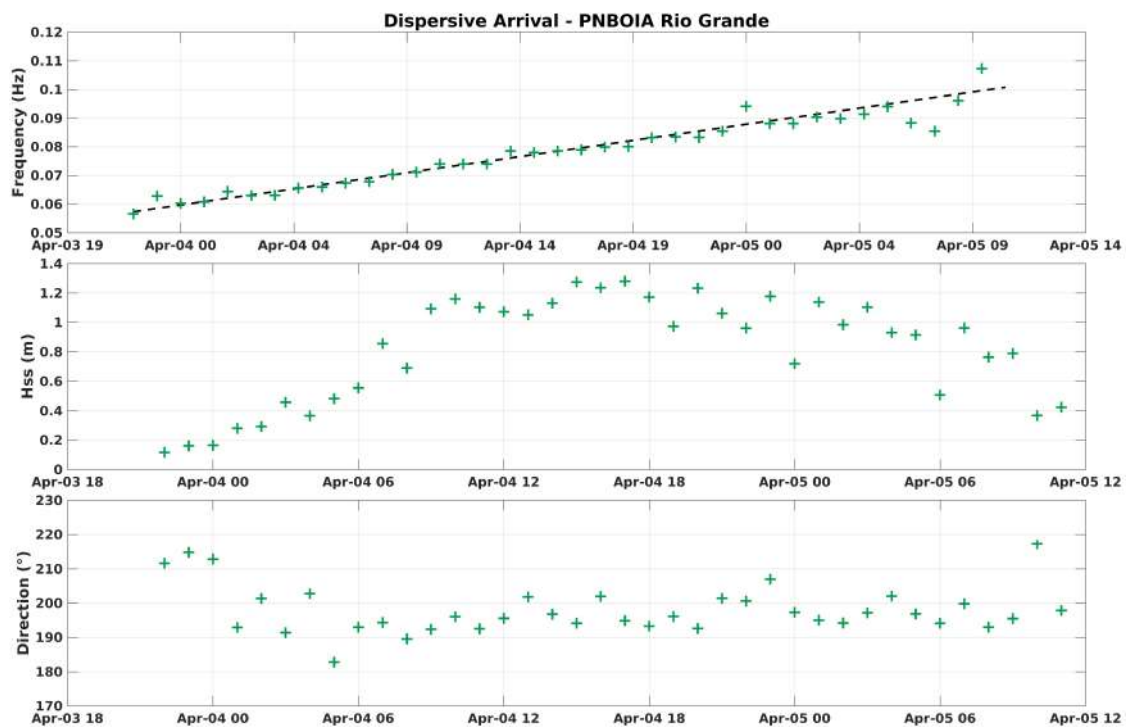
Figure 3.2: Parameters of the dispersive arrival recorded by buoy RG in April 2015, from top to bottom respectively frequency, H_{ss} and direction.
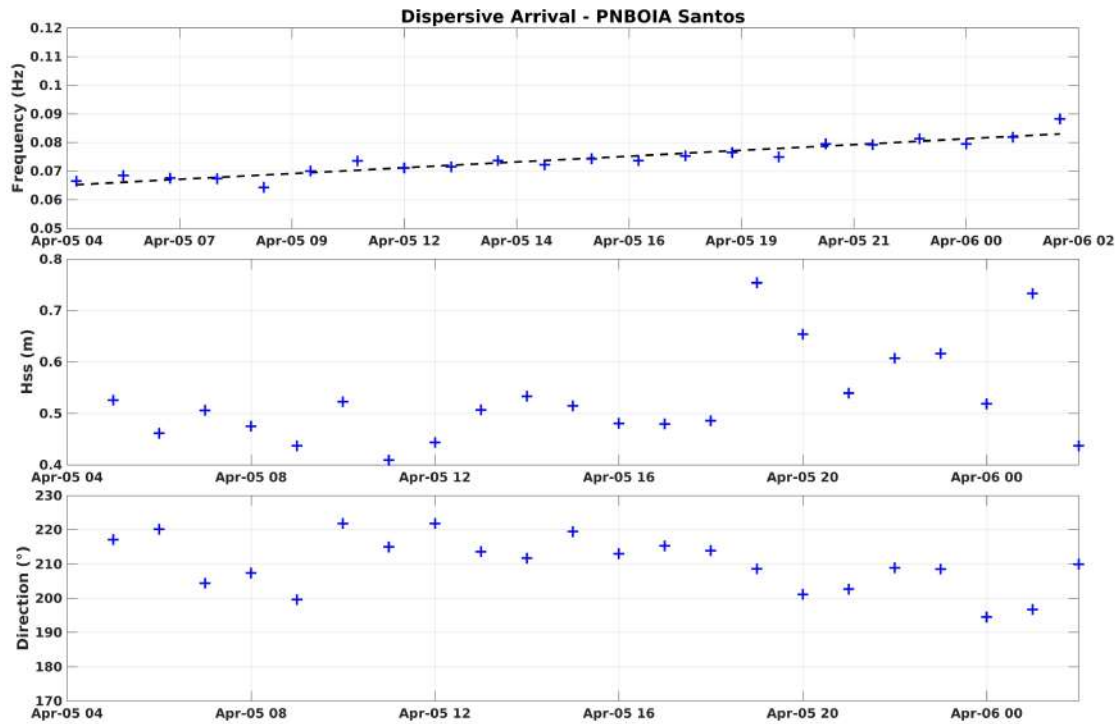
Figure 3.3: Parameters of the dispersive arrival recorded by buoy SA in April 2015, from top to bottom respectively frequency, H_{ss} and direction.

To properly estimate the rate of swell decay, the storm source needs to be located in space and time. Equations 2.2 and 2.3 are employed to track the dispersive waves back to their origin fitting the curves in Figures 3.2 and 3.3. Table 3.1 lists the main computed parameters of the storm center for this event, considering both buoys. The CFSR wind field at 10 m height on the storm estimated date and location is shown in figure 3.4. There is a clear intensification of the wind field near the region pointed out as the swell source. It is also possible to observe the storm's fetch, generating waves that propagate towards both buoys following a path parallel to the trajectory of the great circle. The relative vorticity field estimated using the wind field at 850 hPa presented on figure 3.5 clearly corroborate the estimation of the storm area - the black circle points out the estimated storm radius for April 01, 2015 at 21:00 UTC. Out of the five selected events, this is the one in which the swells were generated the farthest from the buoys.

Table 3.1: Dispersive arrival recorded in April 2015. Distance, date and position of the storm estimated using the data fitting procedure, for both buoys RG and SA.

	Buoy RG	**Buoy SA**
Distance from storm	2395 km	3332 km
Date of the storm	04/01/2015 21 UTC	04/01/2015 23 UTC
Storm's position	-52.78°S / -60.37°W	-49.63°S / -67.89°W
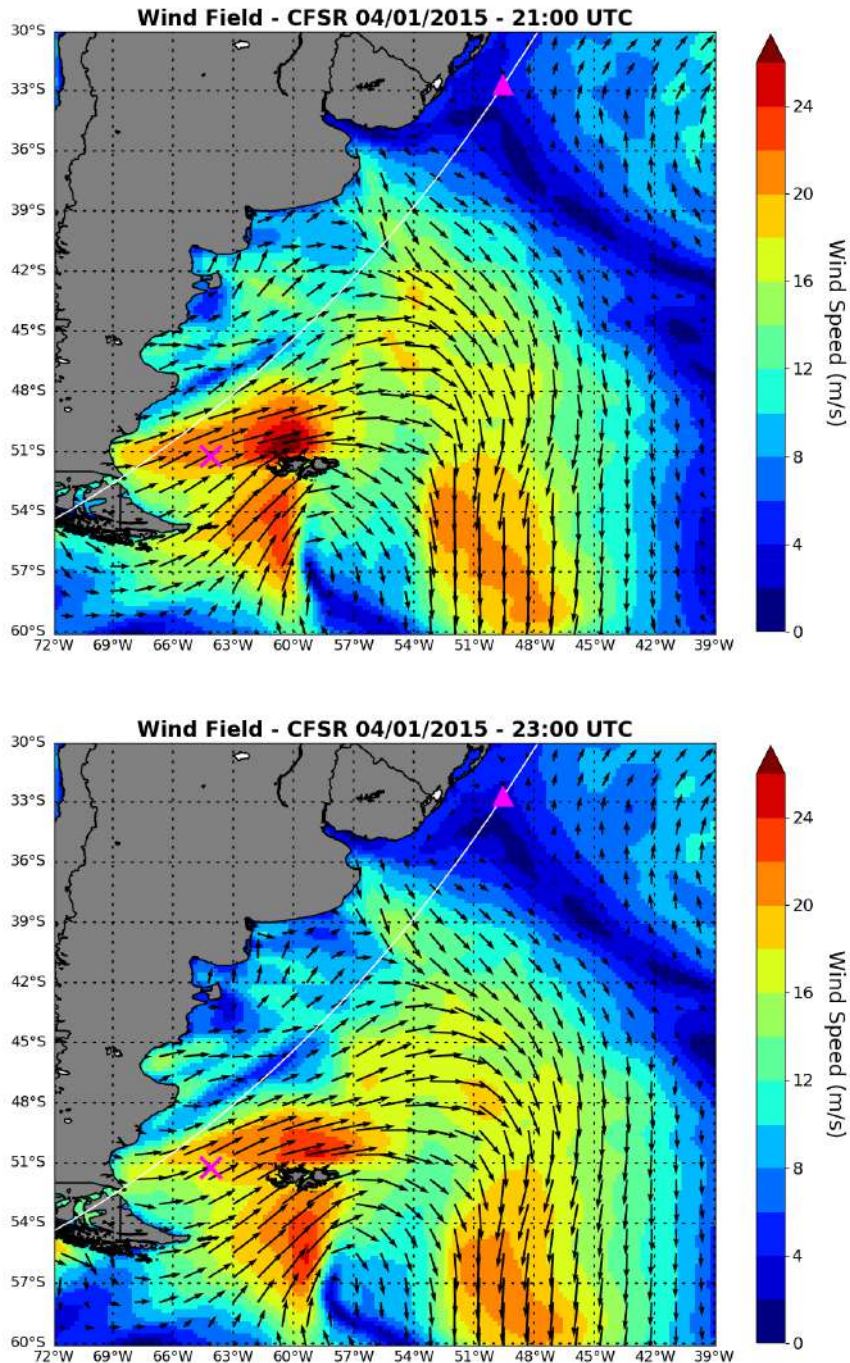
Figure 3.4: Wind field from CFSR on April 1, 2015 at 21:00 UTC (top panel) and 23:00 UTC (bottom panel). The wind speed is represented by the colorbar and direction by arrows. The white line depicts the great circle that passes at the buoys positions. The pink triangle indicates the position of buoy RG and the pink x indicates the average swell source region obtained by dispersive arrival fitting from RG and SA buoys.

15
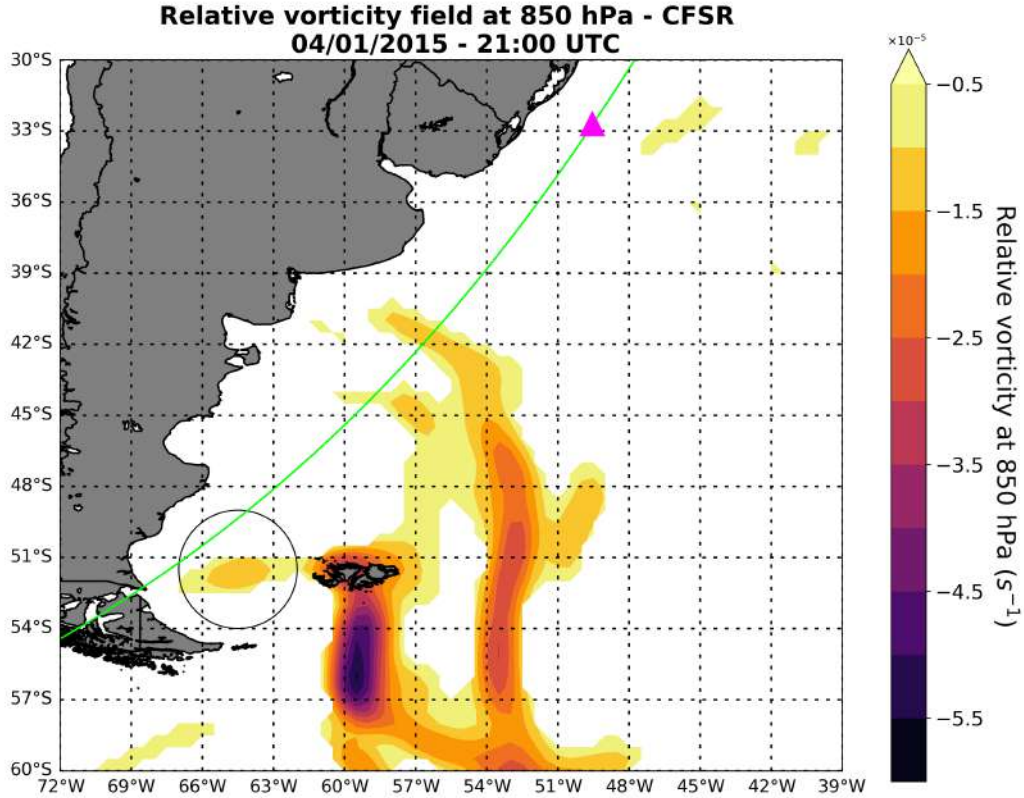
Figure 3.5: Vorticity field estimated using the wind field at 850 hPa from CFSR on April 1, 2015 at 21:00 UTC. The relative vorticity is represented by the colorbar. The green line depicts the great circle that passes at the buoys positions. The pink triangle indicates the position of buoy RG and the black circle indicates the average storm radius estimated using the local maximum of the vorticity field.

3.2 Swell Decay Rate

Table 3.2 shows, for the five selected cases, the computed distances from the buoy RG to the generating storm — hereafter designated as reference distance in the estimations of swell decay — and also the main storm features estimated using the vorticity field at 850 hPa: the storm propagation speed and its diameter. The storm's position of all selected cases is less than 2500 km from buoy RG, with most lying well below the threshold distance assumed in previous works (ARDHUIN *et al.*, 2009; COLLARD *et al.*, 2009; JIANG *et al.*, 2016).

Table 3.2: Reference distances — distance between the estimated storm's position and downwave buoy RG — employed in the computation of swell decay. Also shown the estimated propagation speed and the diameter of the storm estimated using the vorticity field at 850 hPa.

Event	Reference distance	Storm speed	Storm diameter
April 2015	2395 km	23.8 m/s	524 km
June 2014	325 km	11.4 m/s	556 km
June 2012	409 km	19.0 m/s	546 km
May 2012	664 km	20.0 m/s	546 km
March 2012	2007 km	7.6 m/s	556 km

The H_{ss} measured at buoy SA and estimated using the BABANIN (2012) model (top panel) and the linear model (bottom panel) are shown in Figure 3.6. The swell attenuation coefficient $b1$ from equation 2.8 was adjusted for each of the five selected events and the values are presented in table 3.3. With the formulation presented in BABANIN (2012), the computed root mean square error is 0.29 m, with scatter index of 20% and bias of 0.009 m for all 77 measurements. The performance of the linear attenuation model presented in ARDHUIN *et al.* (2009) is not as good — root mean square error is 0.48 m, with scatter index of 33% and bias of 0.23 m.

For the BABANIN (2012) model, as shown in table 3.3, the smaller scatter index (8%) was computed in the event of June 2014, the one with the smallest reference distance. The worst scatter indexes (21%) are in the event June 2012, with reference distance around 400 km, and May 2012, with reference distance of 660 km. The values of $b1$, with exception of the event April 2015 that is similar to the one reported in YOUNG *et al.* (2013), are one or two orders lower than the values suggested by BABANIN (2012). Although the values of $b1$ reported by JIANG *et al.* (2016) are also lower, ranging from -4.0×10^{-4} to 8.0×10^{-4}, the events June 2012 and March 2012 have $b1$ values even lower. Based on equation 2.9, f_e values for each event are also shown in table 3.3.
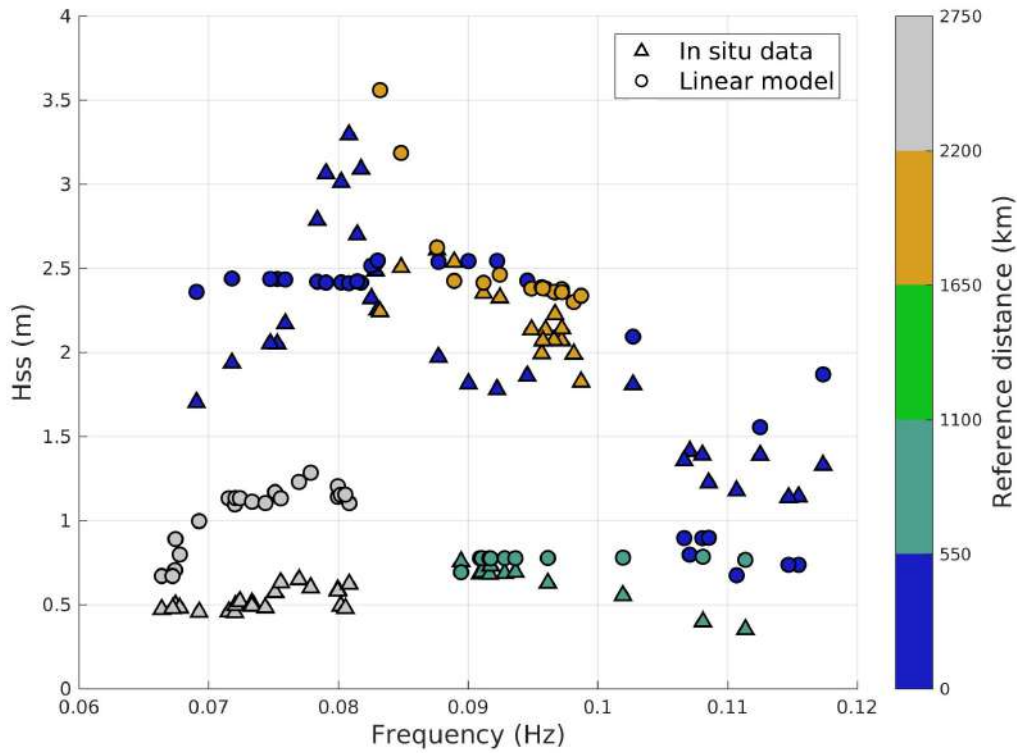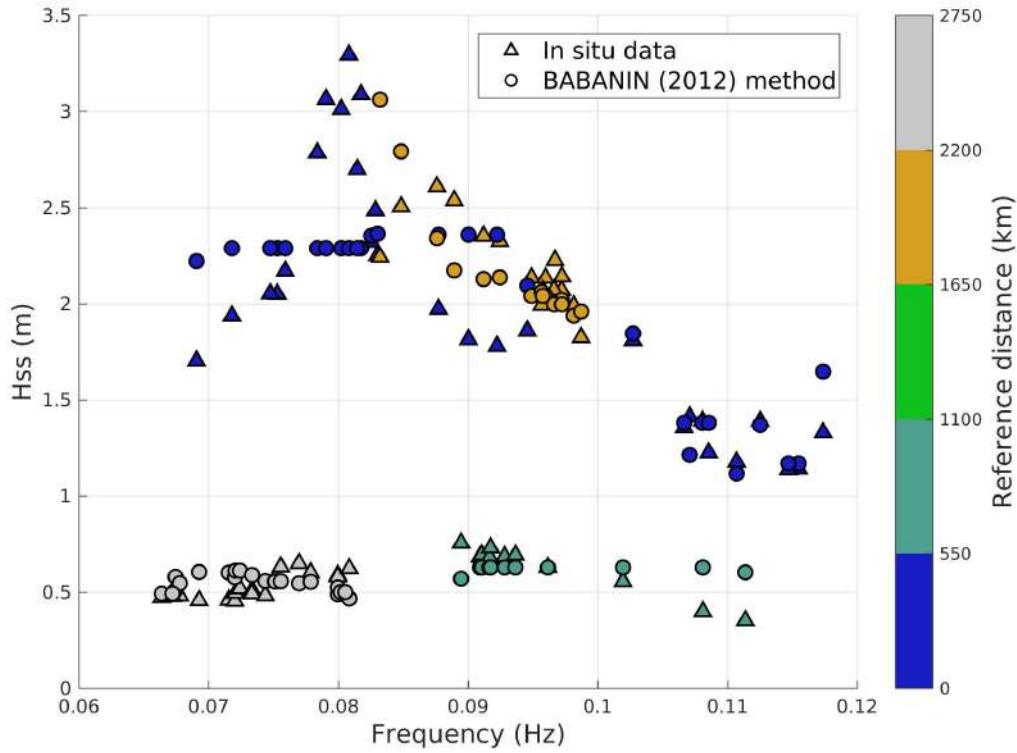
Figure 3.6: Top panel shows the H_{ss} recorded at buoy SA (triangles) and H_{ss} estimated using the BABANIN (2012) formulation (dots) whereas bottom panel shows the H_{ss} recorded in buoy SA (triangles) and H_{ss} estimated using the linear attenuation model presented by ARDHUIN *et al.* (2009) (dots), both for a total of 77 points. The colorbar indicates the reference distance — distance between buoy RG and the storm's estimated position.

Table 3.3: Values of the swell coefficient from the BABANIN (2012) model ($b1$), decay rate (μ_B) and the swell factor from the ARDHUIN *et al.* (2009) nonlinear model (f_e) computed for each swell event. The standard deviation (STD) and scatter index (SI) for μ_B are also shown.

Event	b1	$\overline{\mu_B}$ (m^{-1})	STD (m^{-1})	SI (%)	f_e
April 2015	1.5×10^{-3}	2.1×10^{-6}	3.7×10^{-7}	17	4.9×10^{-2}
June 2014	-4.4×10^{-4}	7.0×10^{-7}	1.9×10^{-8}	8	1.5×10^{-2}
June 2012	7.9×10^{-5}	1.2×10^{-6}	3.3×10^{-8}	21	2.6×10^{-3}
May 2012	2.5×10^{-4}	1.3×10^{-6}	8.1×10^{-9}	21	8.2×10^{-3}
March 2012	5.3×10^{-5}	1.3×10^{-6}	2.4×10^{-8}	12	1.8×10^{-3}

The decay rates μ_B computed in four out of the five events are one order higher than the value of 2.0×10^{-7} reported by SNODGRASS *et al.* (1966), ARDHUIN *et al.* (2009) — which ranges from -0.6×10^{-7} m^{-1} to 3.7×10^{-7} m^{-1} — and JIANG *et al.* (2016), that found decay rates ranging from -1.9×10^{-7} m^{-1} to 4.6×10^{-7} m^{-1}. For the data presented here, the mean μ_B is 1.4×10^{-6} m^{-1} and the median is 1.2×10^{-6} m^{-1}. Therefore, the decay rates in relatively short reference distances are higher.

The top panel of figure 3.7 shows the swell height estimations for event April 2015 using the formulation from BABANIN (2012) – equation 2.8, the linear model (equation 2.5) and the method based on the storm features (SF method — equation 2.12). For this event, the results of the proposed SF method are nearly identical to BABANIN (2012) and both give better results than the linear model. On the other hand, for the events in which the swell source area is located closest to the buoys, the results of the SF method are not accurate, as can be seen in the bottom panel of figure 3.7. Despite this, there is a high correlation of 88% between the data measured by buoy SA and the results obtained using SF method considering all the events together (77 points). The mean decay rate μ_{SF} is 1.9×10^{-6} m^{-1}.
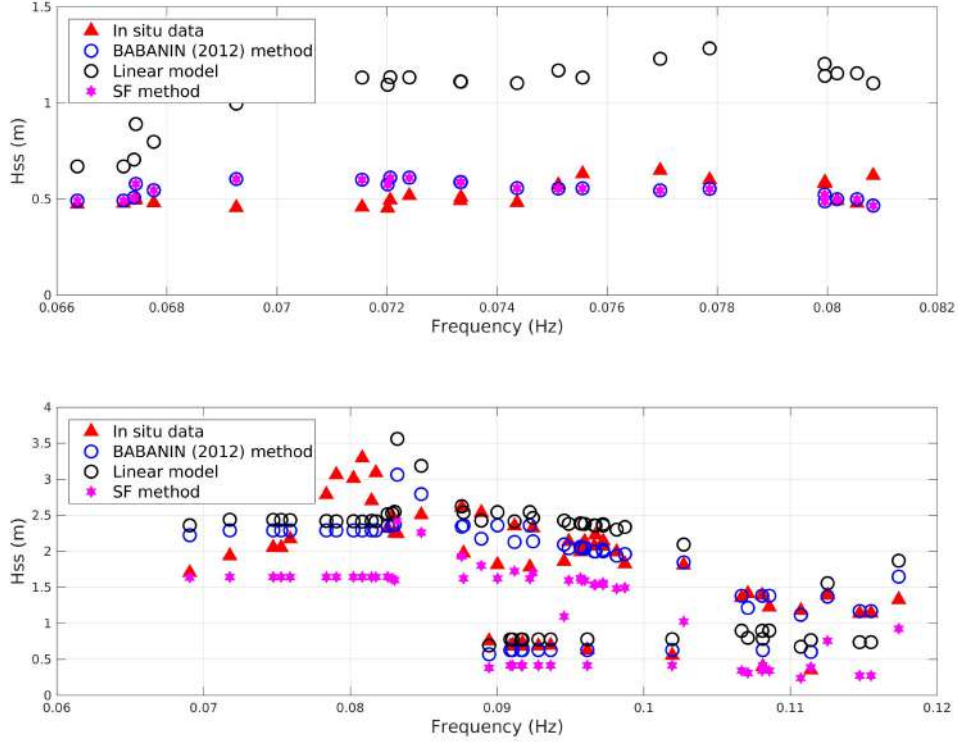
Figure 3.7: Comparison between swell height estimated using the linear model (black circles), the BABANIN (2012) method (blue circles) and the method based on storm features (pink stars) for the event April 2015 (top panel) and the other four events (bottom panel). The red triangles represent the data recorded at buoy SA.

Figure 3.8 shows the ratio between Hss_{SF} and Hss_B. Corroborating the information presented in figure 3.7, the first panel shows that this relation is equal to 1 for the event April 2015. The event June 2014 shows the smallest relationship between Hss_{SF} and Hss_B (0.24), while the other three events exhibits similar relations, with mean ratio equals to 0.71. With the exception of the event April 2015, where the results for Hss_{SF} and Hss_B are equivalent, the proposed SF method underestimates the adjusted values. This fact may indicate that the presented storm features based method shows satisfactory results for swell events generated around 2500 km distant, while for closest ones is necessary more data to fit an adjustment factor in order to get better results for swell decay when applying equation 2.12.
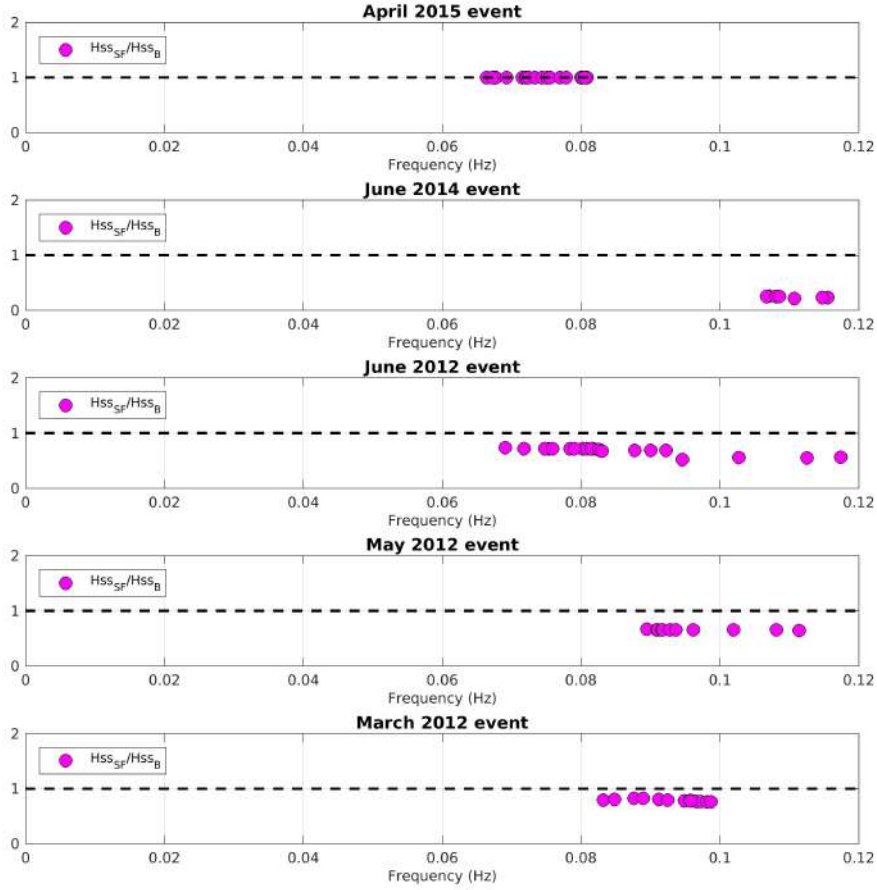
Figure 3.8: Ratio between Hss_{SF}, calculated using the storm feature approach, and Hss_B, estimated using equation 2.7 for each of the five events analyzed. The one-to-one ratio is represented by the dashed line in all subplots.

Considering one swell coefficient $b1$ computed for each event, Figure 3.9 shows the decay rates μ_B. Similar reference distances have different decay rates. Hence, it is clear that the swell decay rate μ_B depends on the reference distance and also on frequency. This is more evident when analysing the event April 2015 — the one more further away from the storm and also the event where the $b1_{SF}$ fits better. This event shows significant variation in frequency. Despite the fact that the reference distance remains naturally the same, there is a considerable variation in the decay rate values. On the other hand, for smaller reference distances, different decay rates are also clear.

21
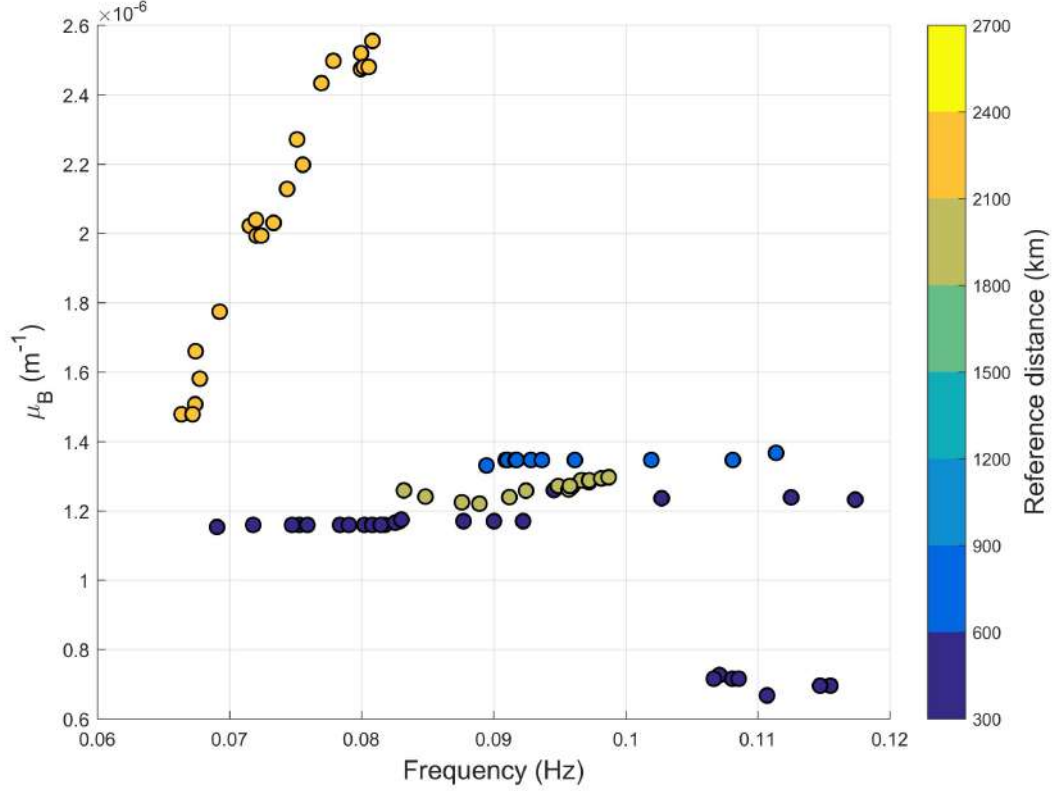
Figure 3.9: Swell decay rate estimated using the model proposed by BABANIN (2012) versus wave frequency. The colourbar indicates the reference distance.

Our results show that, compared to the mentioned previous works (ARDHUIN *et al.*, 2009; BABANIN, 2012; COLLARD *et al.*, 2009; JIANG *et al.*, 2016), the swell decay rate is greater in our measurements — that are relatively closer to the generating storms. Furthermore, although the mean ratio Hss_B/Hss_A is 0.84, it is not constant. This ratio shows a clear dependence on the swell decay rate μ_B (figure 3.10) and the pattern of the relationship between Hss_{SF} and Hss_A suggests a dependence of the swell decay also on the storm features. The Pearson Correlation between the ratio Hss_B/Hss_A and μ_B is equal to -0.895, showing a pattern opposite to the reported in BABANIN (2012). Despite the high linear correlation, here the ratio decreases as a function of μ_B. This may be due to the fact that, in the present study, all events analyzed are closer to the source area than those addressed in the literature. More than that, the observed decay rate here are higher than those presented in other works. It is important to highlight that further investigations are

needed to confirm it. Despite this, as shown by BABANIN (2012), there is a clear underestimation pattern of Hss_B (and also Hss_{SF}) when compared to Hss_A that depends on swell decay rate.
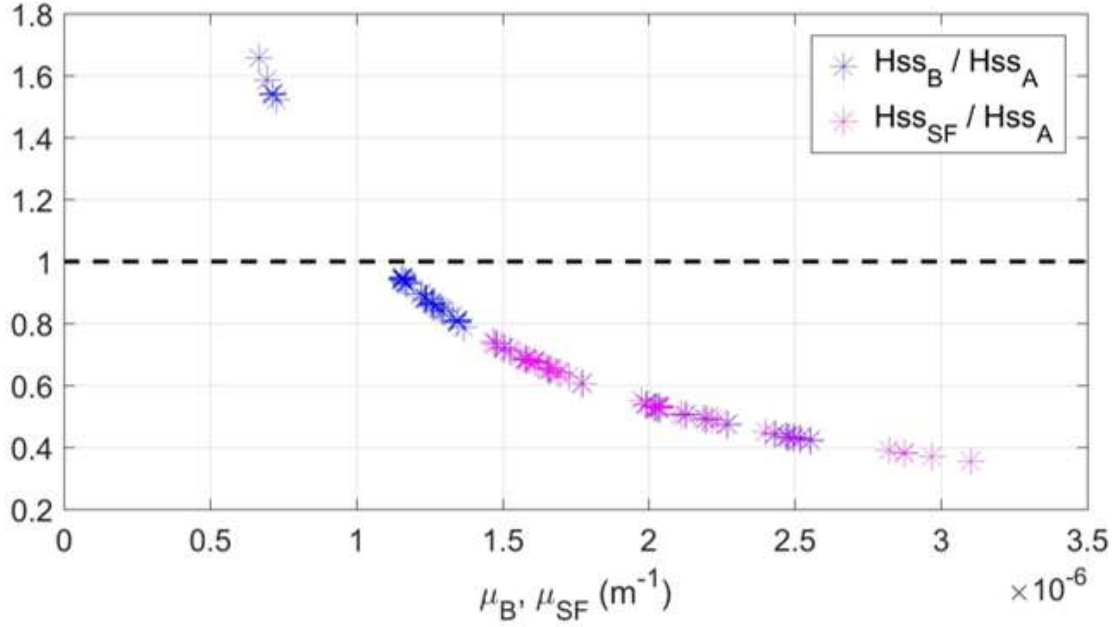
Figure 3.10: Blue asterisks represent the ratio between Hss_B (swell height estimated using the model presented in equation 2.7 for buoy SA) and Hss_A (swell height estimated using ARDHUIN *et al.* (2009)'s linear model), while pink asterisks represent the ratio between Hss_{SF} (swell height estimated using the storm feature approach proposed in equation 2.12 for buoy SA) and Hss_A. The computed dissipation coefficient μ_B μ_{SF} are also shown. The one-to-one ratio is represented by the dashed line.

Chapter 4

Conclusions

The few works that were published in the last decades about swell decay in the ocean were based on satellite data. One, if not the only exception so far, is the classical work by SNODGRASS *et al.* (1966) that employed an array of *in-situ* non-directional wave gauges along a great circle, a cumbersome operation. Undoubtedly, instruments carried on satellites, with the necessary large spatial and temporal coverage, are well suited to investigate the small attenuation of swell energy experienced over thousands of kilometers. The only two satellite instruments able to measure wind waves are the Synthetic Aperture Radar (SAR) and the altimeter — the first Spaceborne Wave Scatterometer has been recently launched and its full capability is yet to be demonstrated.

The considered reference papers about swell decay using remote sensing data (ARDHUIN *et al.*, 2009; COLLARD *et al.*, 2009; JIANG *et al.*, 2016; YOUNG *et al.*, 2013) have employed either SAR or altimeter data, although these instruments have some drawbacks when used to investigate swell decay. The 2D wave directional spectra can be retrieved from SAR images, therefore totally characterizing a sea state. SAR wave spectra have some limitations in the high frequency band while the longer swell waves are better estimated. However, the retrieval of wave spectra from SAR images is a complicated non-linear process prone to inaccuracies, specially in terms of energy content. Significant wave height from altimeters has been demonstrated to be a valuable information, on the other hand. But energy is a

limited piece of information when considering swell decay, and additional data, in general from numerical models, need to be collocated in space and time by presuming several assumptions, which can complicate the procedure.

BABANIN and HAUS (2009), BABANIN (2011) and BABANIN (2012), on the other hand, analysed swell decay using wave tank data and numerical simulations. BABANIN and HAUS (2009) have shown that the decay rate of monochromatic waves generated in tanks is proportional to a^3. Using the same monochromatic-wave experiment, the formulation proposed by BABANIN (2012) is similar to the one presented in ARDHUIN $et\ al.$ (2009). As the laboratory experiment does not impose a distance threshold from the swell source area, this method is tested in the present work using in situ data.

Here, two directional buoys moored 915 km away are employed to investigate swell decay along their great circle. Unlike previous works focused on measurements obtained thousands of kilometers away from the generating storm, five selected cases relatively closer are analysed — all with distances less than 2500 km between the storm and the downwave buoy. Two formulations presented in the literature for swell decay are evaluated. One is a distance-only dependent relation, based on a collection of SAR data (ARDHUIN $et\ al.$, 2009), and the other one is a distance-frequency dependent relation estimated using data from a wave tank (BABANIN, 2012). In addition, a proposed method for swell decay based on the characteristics of the storm is presented and these results were also evaluated.

The distance-frequency dependent relation by BABANIN (2012) is better suited to our data, when the proposed tuning coefficient is corrected to the oceanic conditions. The values of $b1$ here discussed are two orders of magnitude smaller than those proposed in BABANIN (2012), using wave tank data. Moreover, the swell decay in relatively short distances obtained using the frequency-distance dependent model is one order of magnitude lower than the values reported in ARDHUIN $et\ al.$ (2009) and JIANG $et\ al.$ (2016), which imposed as a selection criterion distances larger than the ones here described. BABANIN (2012), in his experiment in a wave

tank, also found decay rates one order lower than the ones here reported. The mean decay rate μ_B found here is $1.4 \times 10^{-6} m^{-1}$ and based on our data, it is indirect inferred from BABANIN (2012) approach that the swell decay is not only dependent on distance but also on wave frequency.

The proposed method dependent on storm features produced equivalent results to those obtained using distance-frequency dependent relation by BABANIN (2012) for the event whose reference distance is about 2400 km, while a great underestimation was obtained for the event closest to the swell source. When an adjustment factor is added to equation 2.11 (not shown), the SF method is capable of representing more accurately the events which the swell source are closer. This may indicate that the storm feature based method (without any adjustment factor) can perform well to calculate swell decay in events in which the reference distance is of around 2500 km, while for closest ones an adjustment factor is necessary for equation 2.11. In that sense, some formulations to compute swell decay have been proposed at the moment in the literature, therefore the results here reported are relevant to increase the knowledge about swell propagation and also for wave numerical modeling progress.

Bibliography

ARDHUIN, F., CHAPRON, B., COLLARD, F., 2009, "Observation of swell dissipation across oceans", *Geophysical Research Letters*, v. 36, n. 6.

BABANIN, A. V., 2012, "Swell attenuation due to wave-induced turbulence". In: *31st International Conference On Ocean, Offshore and Arctic Engineering Division*, v. Volume 2: Structures, Safety and Reliability, *International Conference on Offshore Mechanics and Arctic Engineering*, pp. 439–443, 07.

BABANIN, A. V., JIANG, H., 2017, "Ocean Swell: How Much Do We Know". In: *International Conference on Offshore Mechanics and Arctic Engineering*, v. 3A: Structures, Safety and Reliability, *International Conference on Offshore Mechanics and Arctic Engineering*, 06.

BABANIN, A., 2011, *Breaking and Dissipation of Ocean Surface Waves*. Cambridge, Cambridge University Press. doi: 10.1017/CBO9780511736162.

BABANIN, A. V., HAUS, B. K., 2009, "On the Existence of Water Turbulence Induced by Nonbreaking Surface Waves", *Journal of Physical Oceanography*, v. 39, n. 10, pp. 2675–2679.

CAMPOS, R. M., SOARES, C. G., 2017, "Assessment of three wind reanalyses in the North Atlantic Ocean", *Journal of Operational Oceanography*, v. 10, n. 1, pp. 30–44.

COLLARD, F., ARDHUIN, F., CHAPRON, B., 2009, "Monitoring and analysis of ocean swell fields from space: New methods for routine observations", *Journal of Geophysical Research: Oceans*, v. 114, n. C7.

FLAOUNAS, E., KOTRONI, V., LAGOUVARDOS, K., et al., 2014, "CycloTRACK (v1.0) – tracking winter extratropical cyclones based on relative vorticity: sensitivity to data filtering and other relevant parameters", *Geoscientific Model Development*, v. 7, n. 4, pp. 1841–1853. doi: 10.5194/gmd-7-1841-2014. Disponível em: <https://gmd.copernicus.org/articles/7/1841/2014/>.

GERLING, T. W., 1992, "Partitioning Sequences and Arrays of Directional Ocean Wave Spectra into Component Wave Systems", *Journal of Atmospheric and Oceanic Technology*, v. 9, n. 4, pp. 444–458.

HANSON, J. L., PHILLIPS, O. M., 2001, "Automated Analysis of Ocean Surface Directional Wave Spectra", *Journal of Atmospheric and Oceanic Technology*, v. 18, n. 2, pp. 277–293.

HASSELMANN, K., BRUNING, C., HASSELMANN, K., et al., 1996, "An improved algorithm for the retrieval of ocean wave spectra from synthetic aperture radar image spectra", *Journal of Geophysical Research: Oceans*, v. 101, n. C7, pp. 16615–16629.

HASSELMANN, K., CHAPRON, B., AOUF, L., et al., 2012, "The ERS SAR Wave Mode - A Breakthrough in global ocean wave observations", *European Space Agency, (Special Publication) ESA SP*, v. 1326.

HAUSER, D., TISON, C., AMIOT, T., et al., 2017, "SWIM: The First Spaceborne Wave Scatterometer", *IEEE Transactions on Geoscience and Remote Sensing*, v. 55, n. 5, pp. 3000–3014.

JIANG, H., STOPA, J. E., WANG, H., et al., 2016, "Tracking the attenuation and nonbreaking dissipation of swells using altimeters", *Journal of Geophysical Research: Oceans*, v. 121, n. 2, pp. 1446–1458.

LINDSAY, R., WENSNAHAN, M., SCHWEIGER, A., et al., 2014, "Evaluation of Seven Different Atmospheric Reanalysis Products in the Arctic", *Journal of Climate*, v. 27, n. 7, pp. 2588–2606.

NEU, U., AKPEROV, M. G., BELLENBAUM, N., et al., 2013, "IMILAST: A Community Effort to Intercompare Extratropical Cyclone Detection and Tracking Algorithms: ", *Bulletin of the American Meteorological Society*, v. 94, n. 4 (04), pp. 529–547. ISSN: 0003-0007. doi: 10.1175/BAMS-D-11-00154.1. Disponível em: <https://doi.org/10.1175/BAMS-D-11-00154.1>.

PEREIRA, H. P. P., VIOLANTE-CARVALHO, N., NOGUEIRA, I. C. M., et al., 2017, "Wave observations from an array of directional buoys over the southern Brazilian coast", *Ocean Dynamics*, v. 67, n. 12, pp. 1577–1591.

PIANCA, C., MAZZINI, P. L. F., SIEGLE, E., 2010, "Brazilian offshore wave climate based on NWW3 reanalysis", *Brazilian Journal of Oceanography*, v. 58, pp. 53–70.

PORTILLA-YANDÚN, J., VALLADARES, C., VIOLANTE-CARVALHO, N., 2019, "A Hybrid Physical-Statistical Algorithm for SAR Wave Spectra Quality Assessment", *IEEE Journal of Selected Topics in Applied Earth Observations and Remote Sensing*, v. 12, n. 10, pp. 3943–3948.

RIBAL, A., YOUNG, I. R., 2019, "33 years of globally calibrated wave height and wind speed data based on altimeter observations", *Scientific Data*, v. 6, n. 1, pp. 1–15.

SAHA, S., MOORTHI, S., PAN, H.-L., et al., 2010, "The NCEP Climate Forecast System Reanalysis", *Bulletin of the American Meteorological Society*, v. 91, n. 8, pp. 1015–1058.

SHARP, E., DODDS, P., BARRETT, M., et al., 2015, "Evaluating the accuracy of CFSR reanalysis hourly wind speed forecasts for the UK, using in situ measurements and geographical information", *Renewable Energy*, v. 77, pp. 527 – 538.

SNODGRASS, F. E., GROVES, G. W., HASSELMANN, K. F., et al., 1966, "Propagation of Ocean Swell across the Pacific", *Philosophical Transactions of the Royal Society of London*, v. 259, n. 1103, pp. 431–497.

VIOLANTE-CARVALHO, N., OCAMPO-TORRES, F. J., ROBINSON, I. S., 2004, "Buoy observations of the influence of swell on wind waves in the open ocean", *Applied Ocean Research*, v. 26, n. 1, pp. 49–60.

VIOLANTE-CARVALHO, N., ROBINSON, I. S., SCHULZ-STELLENFLETH, J., 2005, "Assessment of ERS synthetic aperture radar wave spectra retrieved from the Max-Planck-Institut (MPI) scheme through intercomparisons of 1 year of directional buoy measurements", *Journal of Geophysical Research: Oceans*, v. 110, n. C7.

YOUNG, I. R., BABANIN, A. V., ZIEGER, S., 2013, "The Decay Rate of Ocean Swell Observed by Altimeter", *Journal of Physical Oceanography*, v. 43, n. 11, pp. 2322–2333.

Appendix A

Swell arrival events

A.1   June 2014 event

Figure A.1 shows spectograms for the dispersive arrival event on June 2014. In both spectograms is possible to see that swell energy here is concentrated in higher frequencies if compared with the event occurred on April 2015 (see section 3.1), which indicates this swell system was generated in a closer region. Here swell system seems to dominate all wave spectrum and the migration of swell energy towards slightly higher frequencies over time is not so clear on the spectograms.
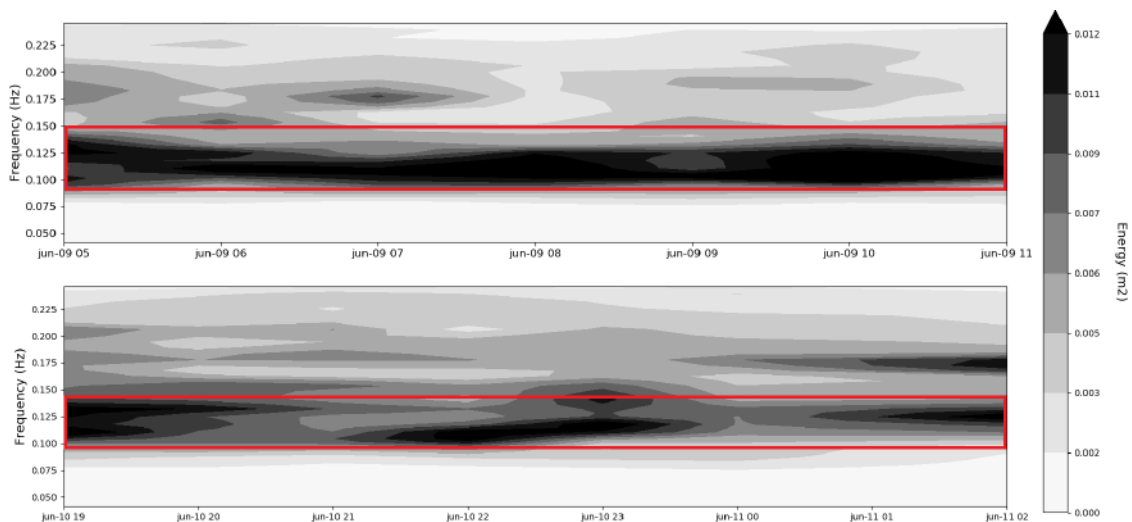

Figure A.1: Evolution of the non-directional spectra over time during the dispersive arrival event recorded at buoy RG (top panel) and buoy SA (bottom panel) on June 2014. The red box highlights the evolution of swell field on the spectra over time.

Figures A.2 and A.3 show the dispersive pattern of swell system recorded at buoy RG and buoy SA, respectively. Despite the small amount of data, the trend of increasing the frequency of the swell over time is now clear.
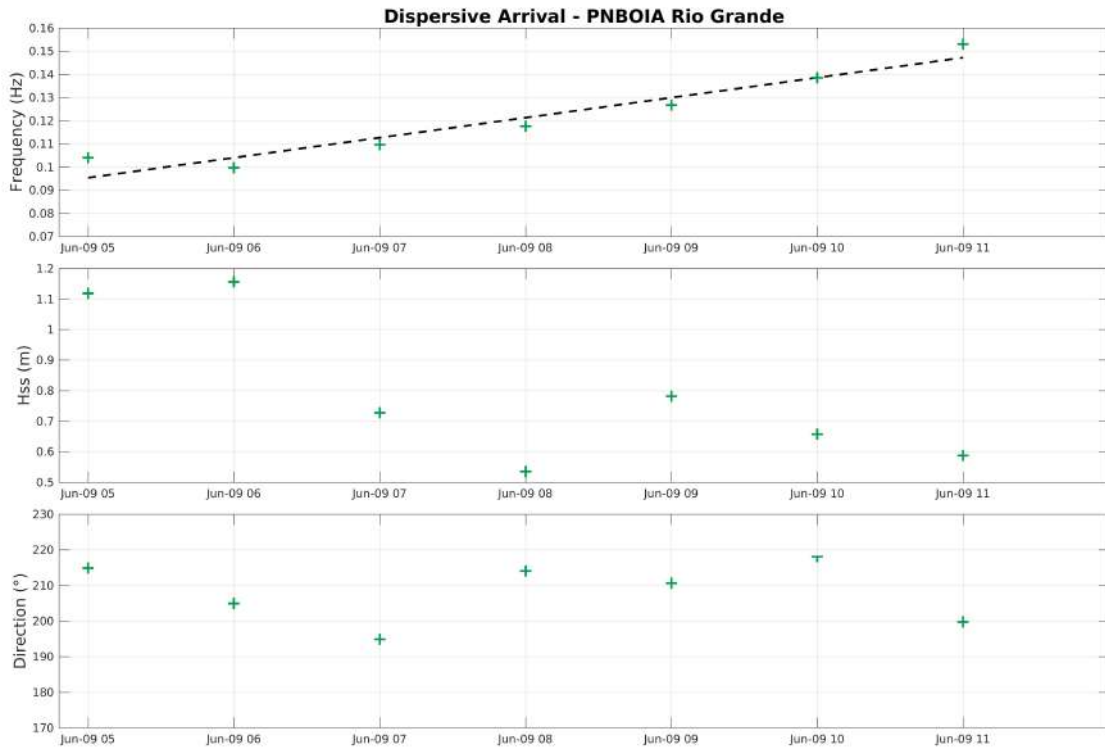

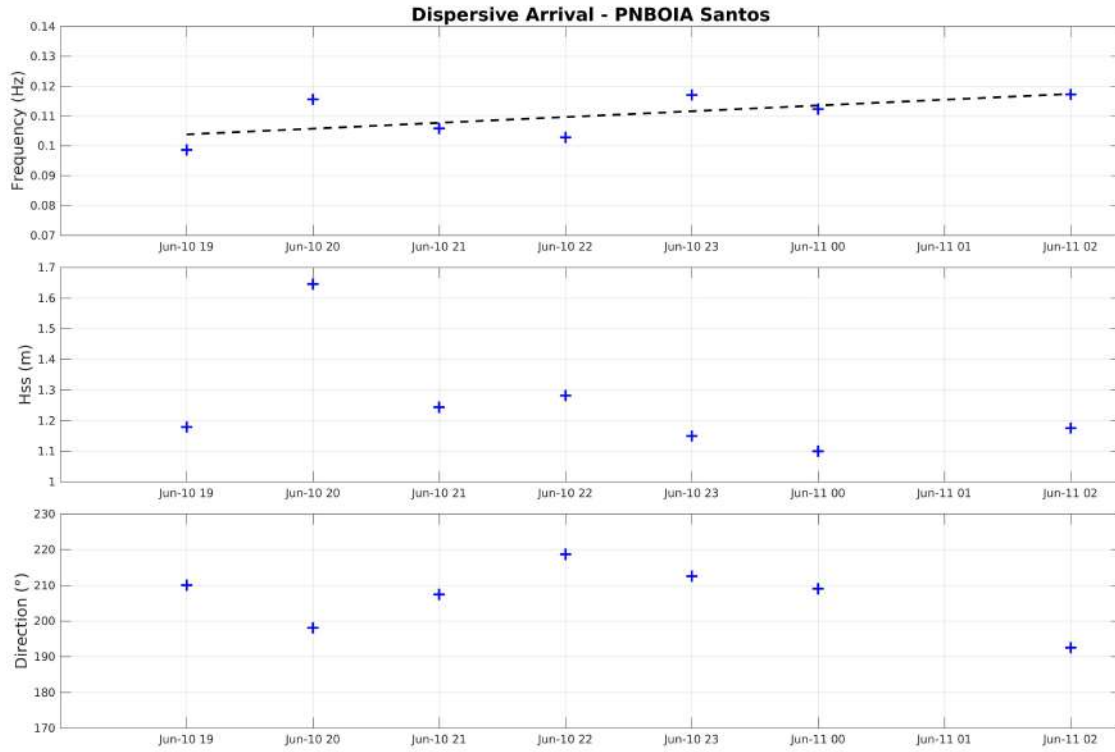Figure A.2: Dispersive arrival event recorded at buoy RG on June 2014.

Figure A.3: Dispersive arrival event recorded at buoy SA on June 2014.

The distance from the swell source and the moment when the storm occurred are shown on table A.1. This storm happened in an area very close to RG buoy - the wind field from CFSR can be see in figure A.4. This fact must be taken into account when analyzing the results of swell attenuation, since a storm very close to the buoy's location can still influence the swell energy recorded on the buoys'. The relative vorticity field for June 8, 2014 at 13:00 UTC is shown in figure A.5, corroborating the position of the storm.

Table A.1: Dispersive arrival recorded on June 2014. Distance, date and position of the storm estimated using the data fitting procedure, for both buoys RG and SA.

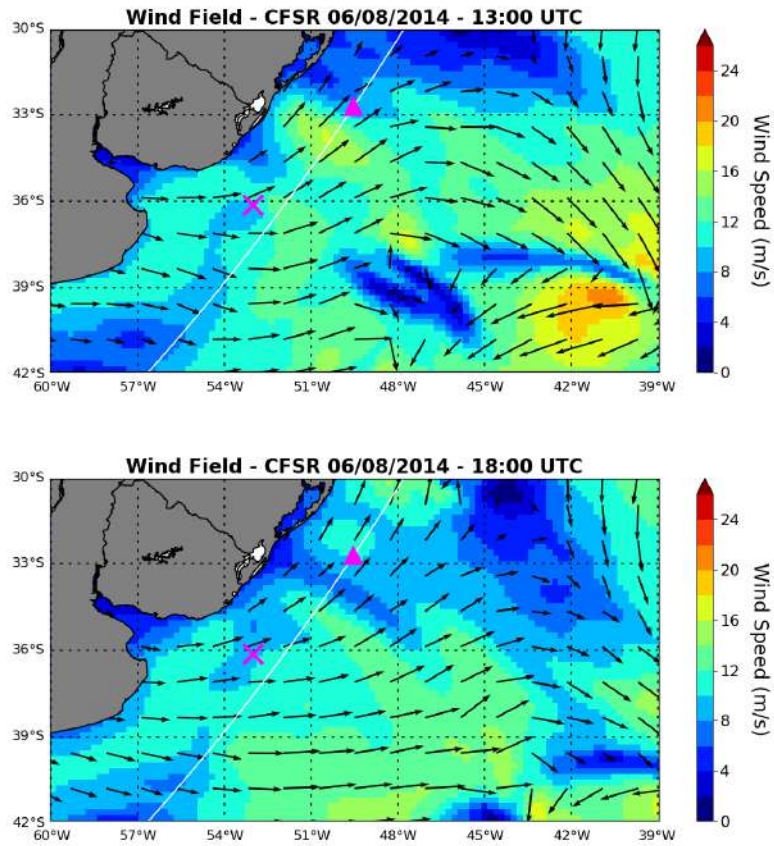|	Buoy RG	Buoy SA
Distance from storm	325 km	1450 km
Date of the storm	06/08/2014 18 UTC	06/08/2014 13 UTC
Storm's position	-36.89°S / -52.37°W	-35.27°S / -51.25°W

Figure A.4: Wind field from CFSR referring to June 8, 2014 at 13 (top panel) and 18 (bottom panel) utc. The wind speed is represented by the colours while the direction is represented by the arrows. The white line shows the trajectory of the great circle that passes through the buoys RG and SA. The pink triangle indicates the buoy RG position and the pink x indicates the average swell source region obtained by dispersive arrival curves from RG and SA buoys.
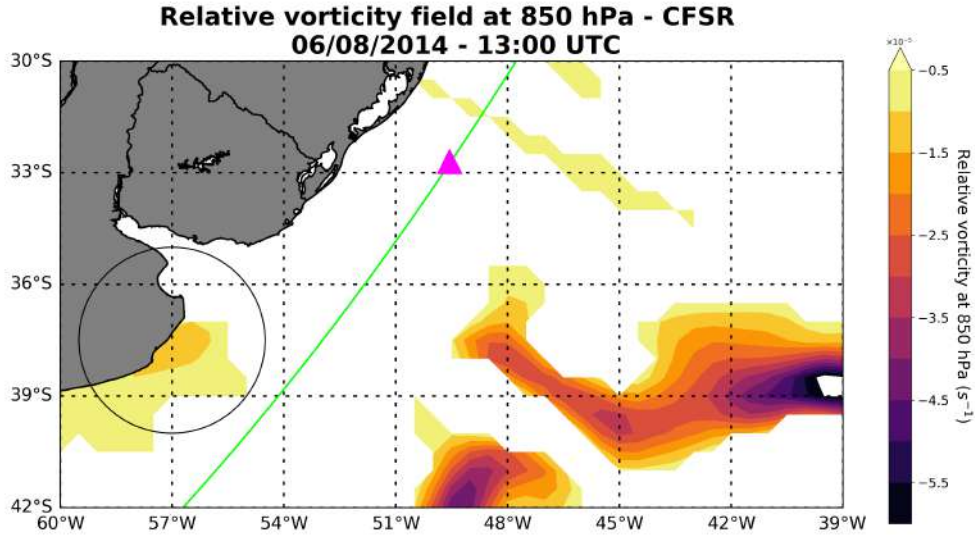
Figure A.5: Vorticity field estimated using wind field at 850 hPa from CFSR on June 8, 2014 at 13:00 UTC. The relative vorticity is represented by the colorbar. The green line depicts the great circle that passes at the buoys positions. The pink triangle indicates the position of buoy RG and the black circle indicates the average storm radius estimated using the local maximum of the vorticity field.

A.2   June 2012 event

Figure A.6 shows spectograms for the dispersive arrival event recorded on June 2012. Contrary to expectations, it can be seen an increase in swell energy in some frequencies on buoy SA records compared to the buoy RG data. This can better be noted in figures A.7 and A.8, where the higher Hss value at buoy RG is around 3 m and the higher Hss at buoy SA is around 3.5 m. Although not expected, under natural conditions the swell growth ("negative attenuation") can occur due to interactions with local winds or local waves during its propagation (BABANIN and JIANG, 2017).
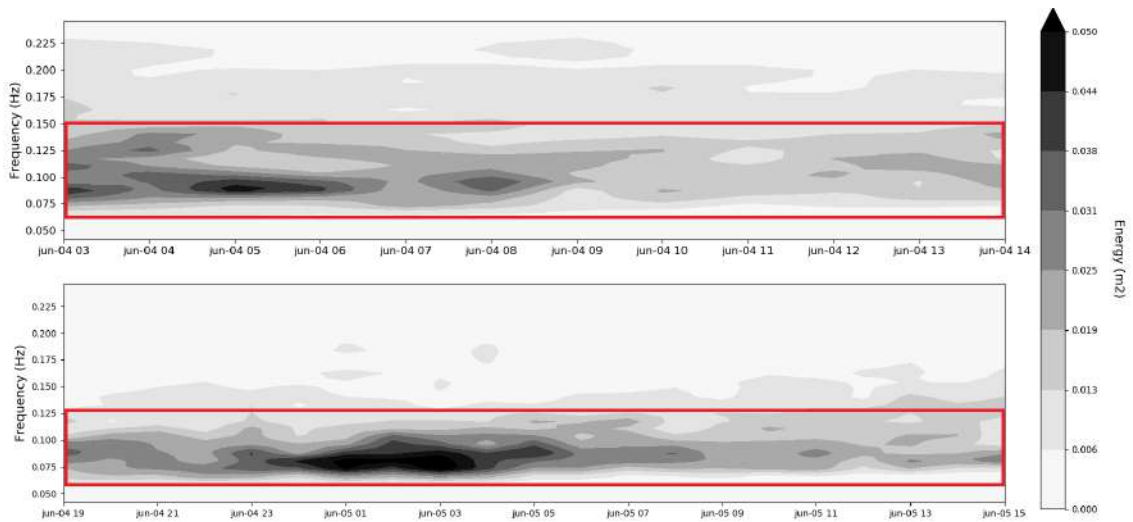
Figure A.6: Evolution of the non-directional spectra over time during the dispersive arrival event recorded at buoy RG (top panel) and buoy SA (bottom panel) on June 2012. The red box highlights the evolution of swell field on the spectra over time.
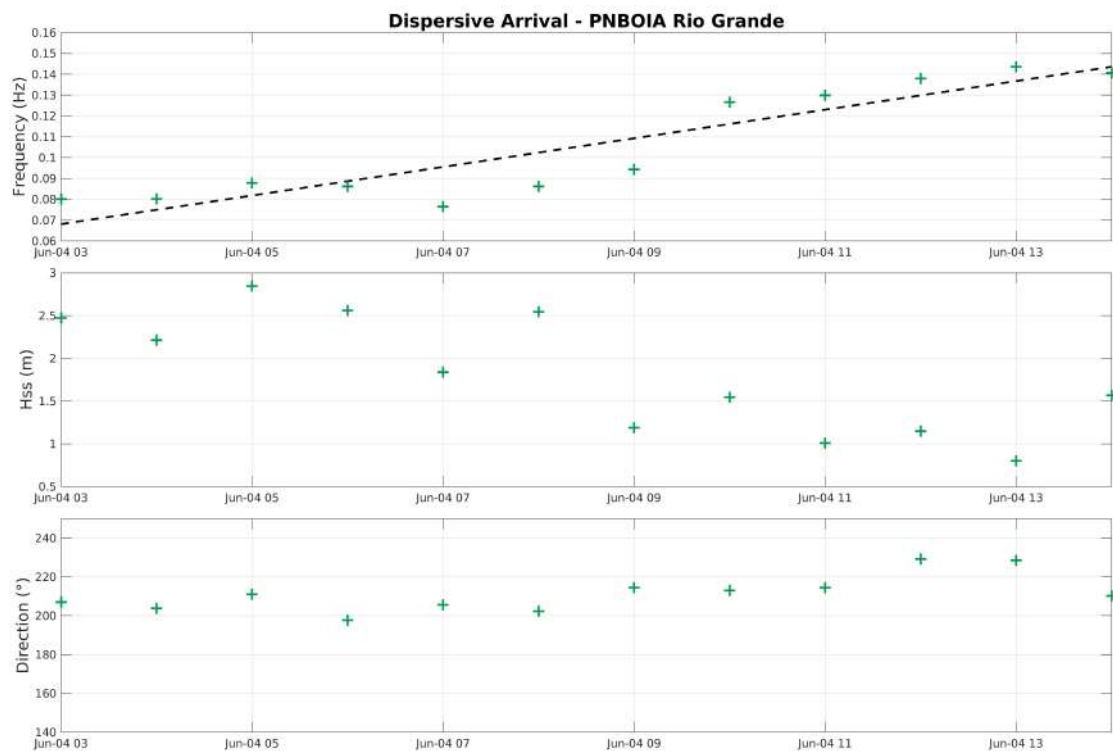

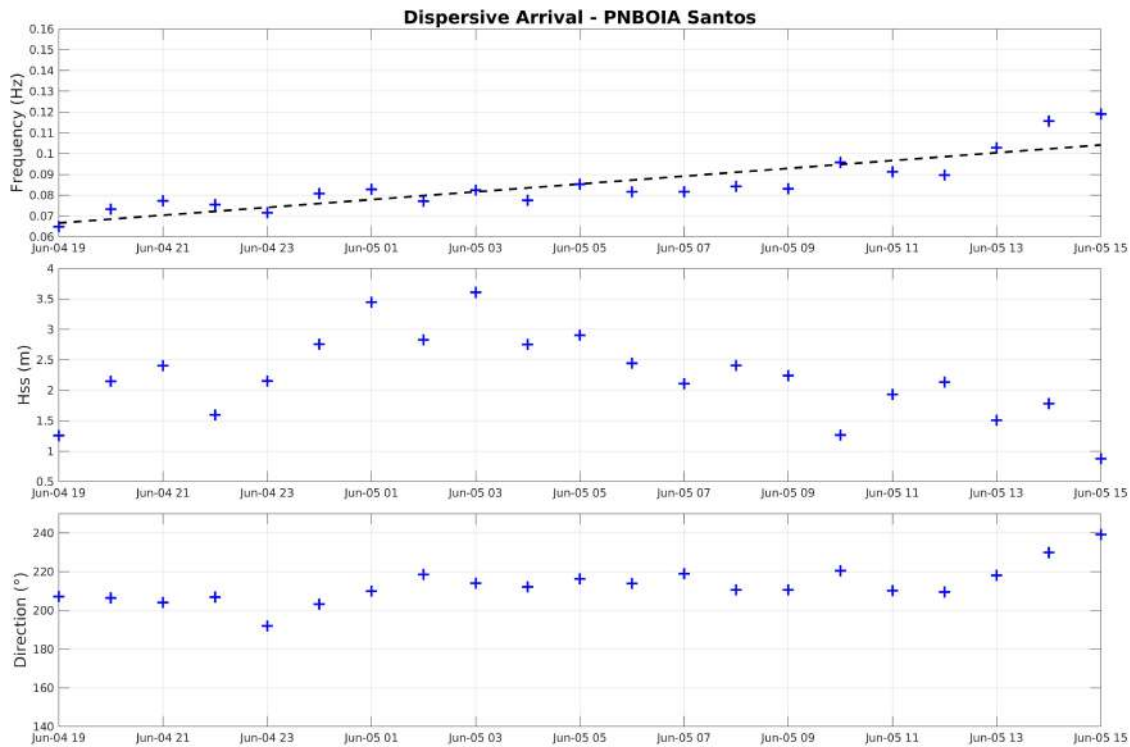Figure A.7: Dispersive arrival event recorded at buoy RG on June 2012.

Figure A.8: Dispersive arrival event recorded at buoy SA on June 2012.

Despite the unexpected increase in Hss values in certain frequencies between the buoy RG and buoy SA, from the information presented on figures A.7 and A.8, it is possible to verify the small difference between swell direction values recorded by the two buoys. So, together with the frequency data, the direction information can corroborate the hypothesis that the records from both buoys refer to swells generated by the same storm.

The distance from the swell source and the moment when the storm occurred are shown on table A.2. Here, the storm possibly responsible to the generation of the waves recorded on this dispersive arrival event is located in an area very close to RG buoy (figure A.9). This information is confirmed by figure A.10, which displays the relative vorticity field. The group velocity (C_g) of the faster swell component (lower frequency) is about 12 m/s, while the mean speed of the storm is around 19 m/s. This indicates that the storm and the waves were propagating at close speeds, which can cause feedback in terms of energy of certain wave frequencies after their generation. As already mentioned, ocean swells have the potential to reconnect with

36

the winds while propagating (BABANIN and JIANG, 2017).

Figure A.9 presentes the wind field from CFSR on June 3, 2012 at 8 (left) and 17 (right) UTC while figure A.10 shows the relative vorticity field at 850 hPa for June 3, 2012 at 08:00 UTC. From both figures, it is possible to note the presence of a huge cyclone. The wind speed at 10 m height reaches up to 22 m/s on a fetch aligned with the great circle path relatively near to buoy RG (pink triangle).

Table A.2: Dispersive arrival recorded on June 2012. Distance, date and position of the storm estimated using the data fitting procedure, for both buoys RG and SA.

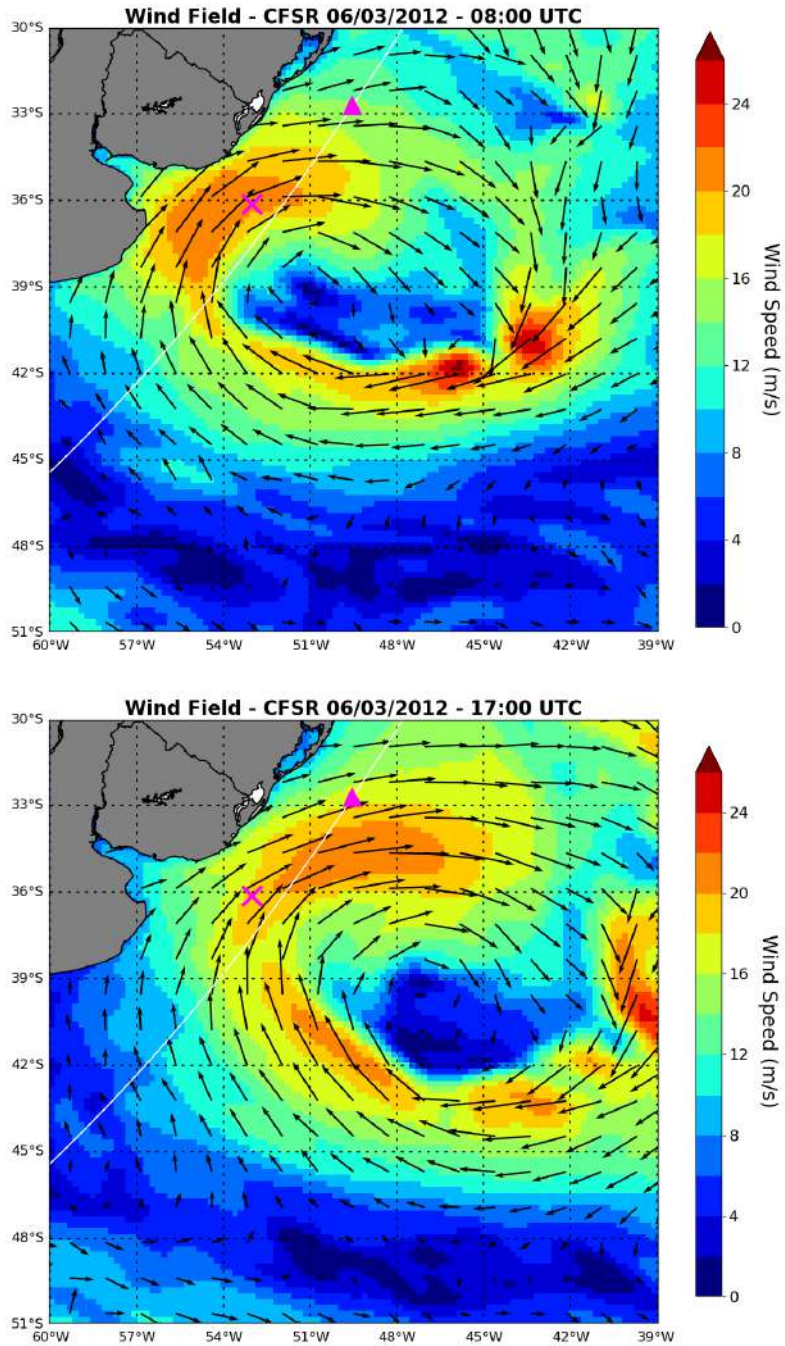|	Buoy RG	Buoy SA
Distance from storm	409 km	1495 km
Date of the storm	06/03/2012 17 UTC	06/03/2012 08 UTC
Storm's position	-35.82°S / -51.93°W	-36.44°S / -54.09°W

Figure A.9: Wind field from CFSR referring to June 3, 2012 at 8 (left panel) and 17 (right panel) UTC. The wind speed is represented by the colours while the direction is represented by the arrows. The white line shows the trajectory of the great circle that passes through the buoys RG and SA. The pink triangle indicates the buoy RG position and the pink x indicates the average swell source region obtained by dispersive arrival curves from RG and SA buoys.
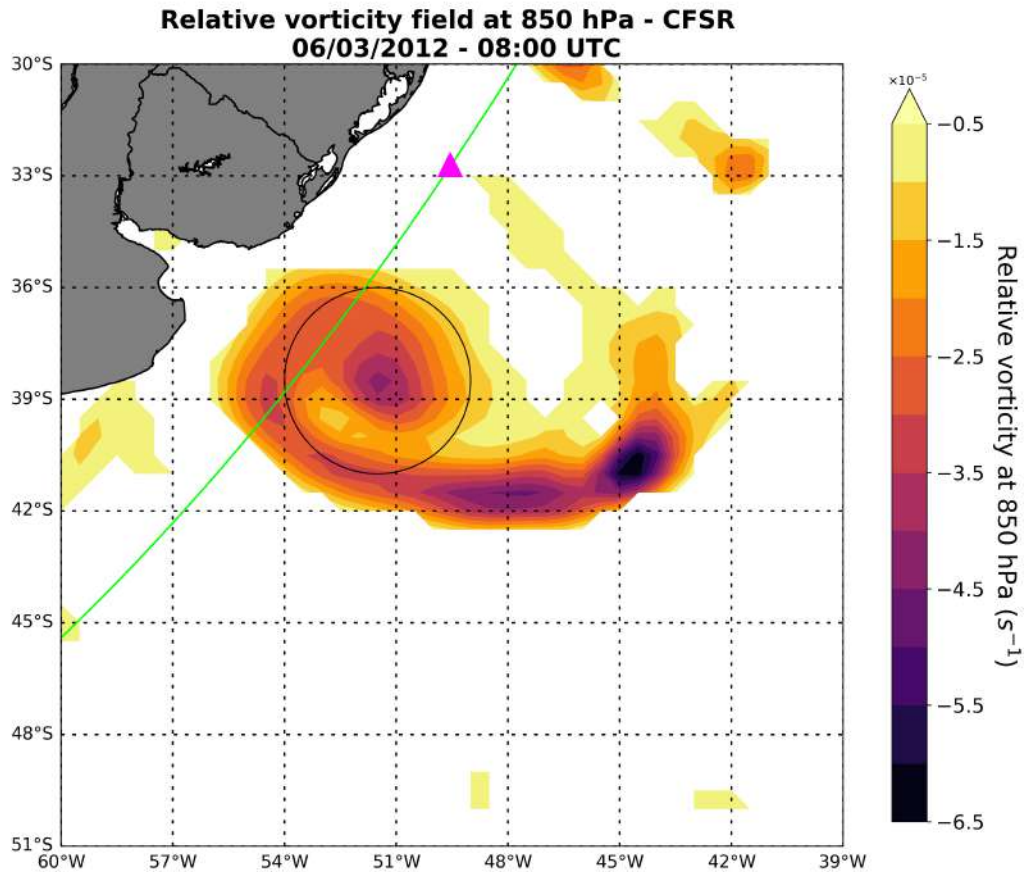
Figure A.10: Vorticity field estimated using wind field at 850 hPa from CFSR on June 3, 2012 at 08:00 UTC. The relative vorticity is represented by the colorbar. The green line depicts the great circle that passes at the buoys positions. The pink triangle indicates the position of buoy RG and the black circle indicates the average storm radius estimated using the local maximum of the vorticity field.

A.3   May 2012 event

Figure A.11 shows spectograms for the dispersive arrival event recorded on May 2012. Although the identification of the swell's dispersive arrival is not very clear in the buoy RG data because of the great amount of energy in high frequencies, the bottom panel clearly shows the dispersive arrival recorded on buoy RG.
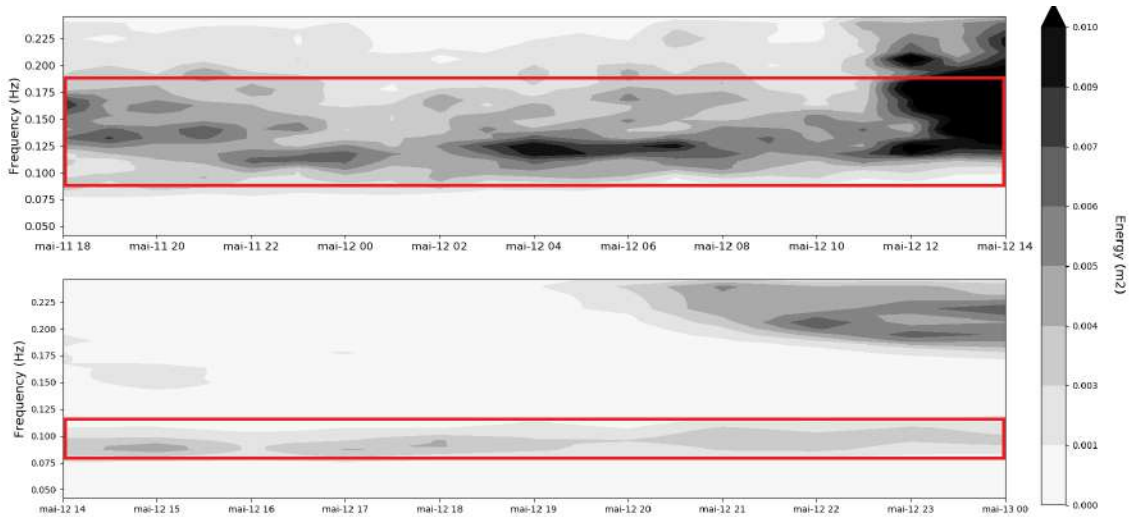
Figure A.11: Evolution of the non-directional spectra over time during the dispersive arrival event recorded at buoy RG (top panel) and buoy SA (bottom panel) on May 2012. The red box highlights the evolution of swell field on the spectra over time.

Figures A.12 and A.13 show the swell arrival recorded by RG and SA buoys, respectively. There is an explicit downward trend in Hss values between buoy RG and buoy SA sites. Besides that, it is possible to see that swell attenuation is greater in higher frequencies than in lower frequencies. It strongly suggests that swell attenuation have some relation with the swell frequency.
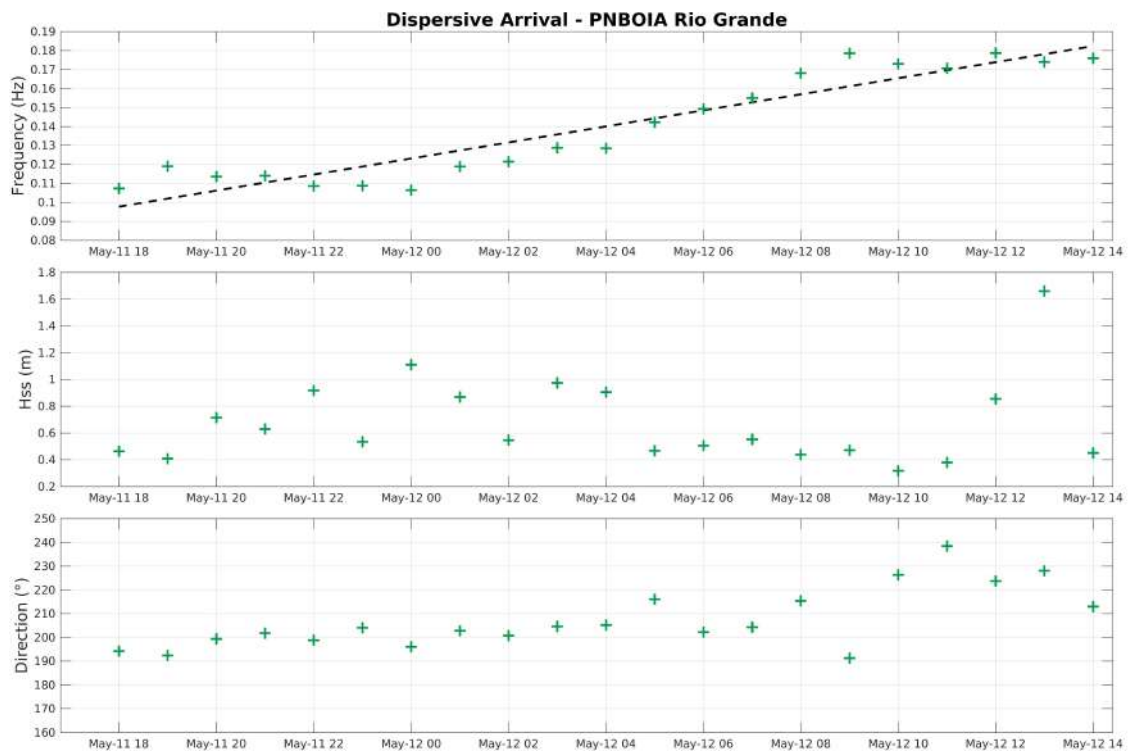

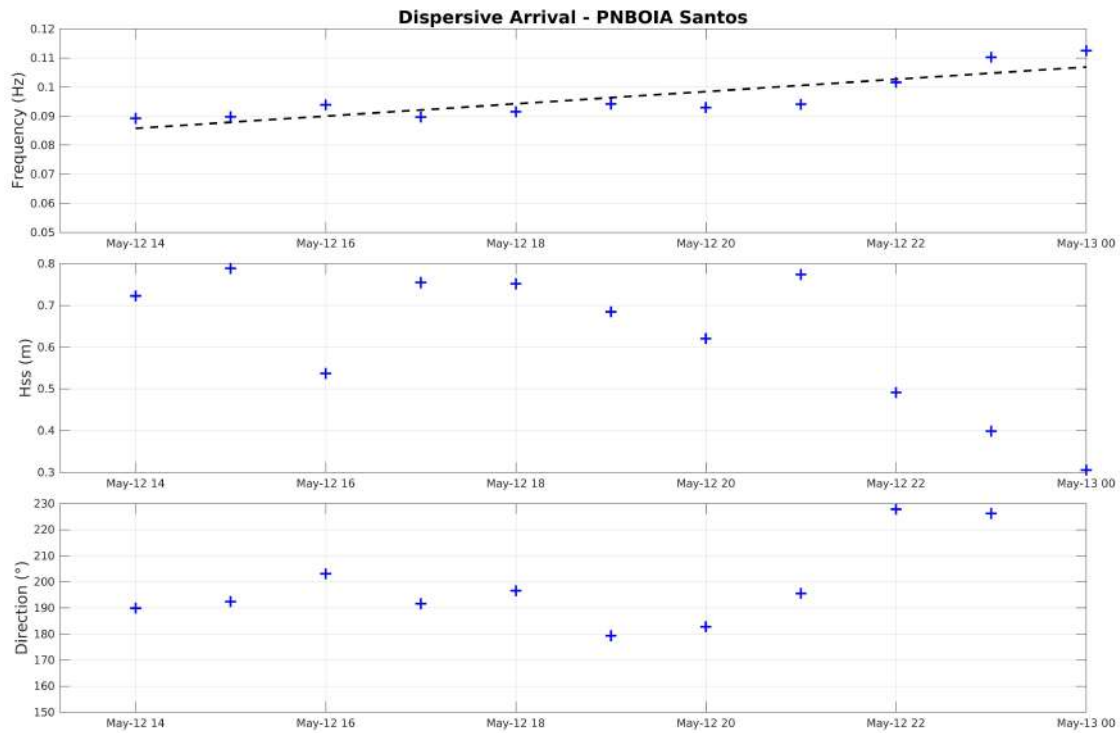Figure A.12: Dispersive arrival event recorded at buoy RG on May 2012.

Figure A.13: Dispersive arrival event recorded at buoy SA on May 2012.

The distance from the swell source and the moment when the storm occurred as calculated from the fitted curves are shown on table A.3. Figure A.14 and A.15 illustrate the proximity of the storm with the buoy RG. Although the cyclogenesis area is relatively close to buoy RG, the cyclone has average dimensions of the order of 546 km and mean speed of around 20 m/s. The atmospheric characteristics could be a reason to explain the fact that there is no clear energy input after swell generation, even with the proximity to the buoy site.

Table A.3: Dispersive arrival recorded on May 2012. Distance, date and position of the storm estimated using the data fitting procedure, for both buoys RG and SA.

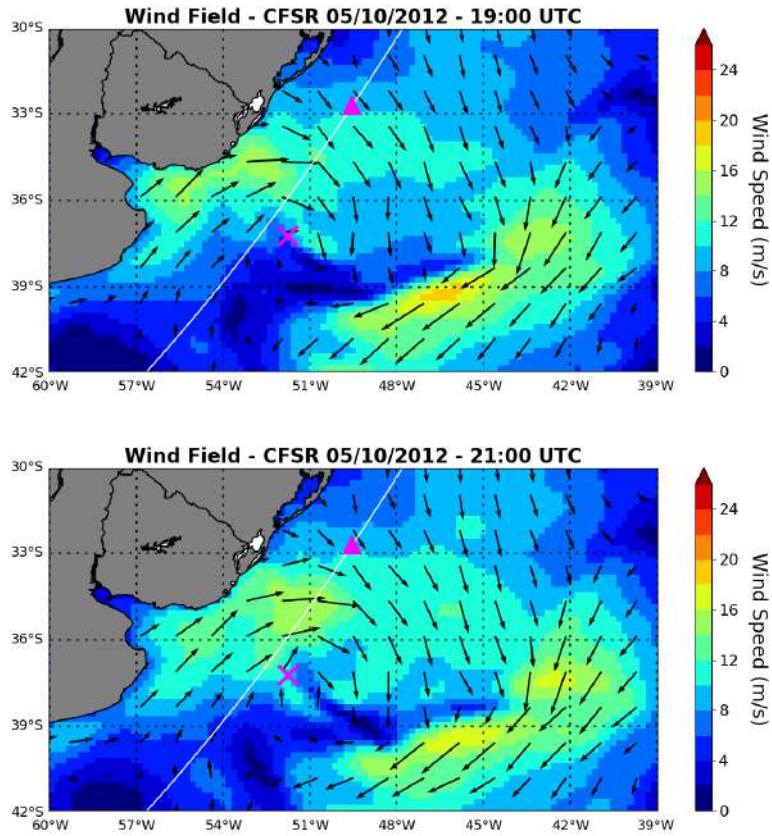|	Buoy RG	Buoy SA
Distance from storm	664 km	1331 km
Date of the storm	05/10/2012 19 UTC	05/10/2012 21 UTC
Storm's position	-57.84°S / -47.35°W	-52.52°S / -47.04°W

Figure A.14: Wind field from CFSR referring to May 10, 2012 at 19 (top panel) and 21 (bottom panel) utc. The wind speed is represented by the colours while the direction is represented by the arrows. The white line shows the trajectory of the great circle that passes through the buoys RG and SA. The pink triangle indicates the buoy RG position and the pink x indicates the average swell source region obtained by dispersive arrival curves from RG and SA buoys.
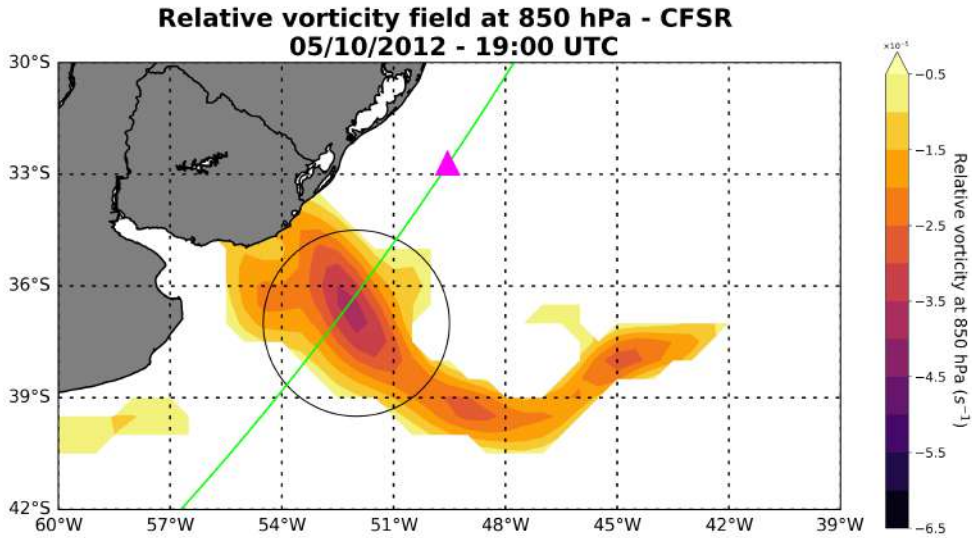
Figure A.15: Vorticity field estimated using wind field at 850 hPa from CFSR on May 10, 2012 at 19:00 UTC. The relative vorticity is represented by the colorbar. The green line depicts the great circle that passes at the buoys positions. The pink triangle indicates the position of buoy RG and the black circle indicates the average storm radius estimated using the local maximum of the vorticity field.

A.4   March 2012 event

Figure A.16 shows spectograms for the dispersive arrival event on March 2012. On both buoys, the swell energy dominates the sea state and the event is clearly identified.
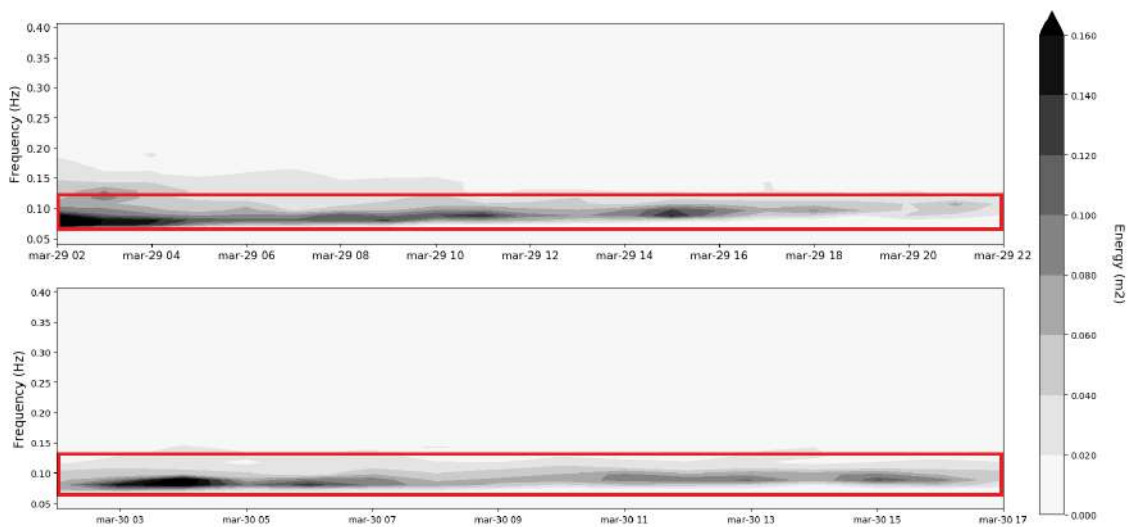

Figure A.16: Evolution of the non-directional spectra over time during the dispersive arrival event recorded at buoy RG (top panel) and buoy SA (bottom panel) on March 2012. The red box highlights the evolution of swell field on the spectra over time.

Figures A.17 and figure A.18 show an obvious trend for Hss to decrease over time in each site. This decrease is also noted when buoy RG data is compared to buoy SA data, which indicates there is a swell energy attenuation between buoy RG and buoy SA. As this is a more distant generated swell arrival event (as presented on table A.4), the attenuation behavior of the swell energy as the waves propagate over greater distances is more clearly observed.
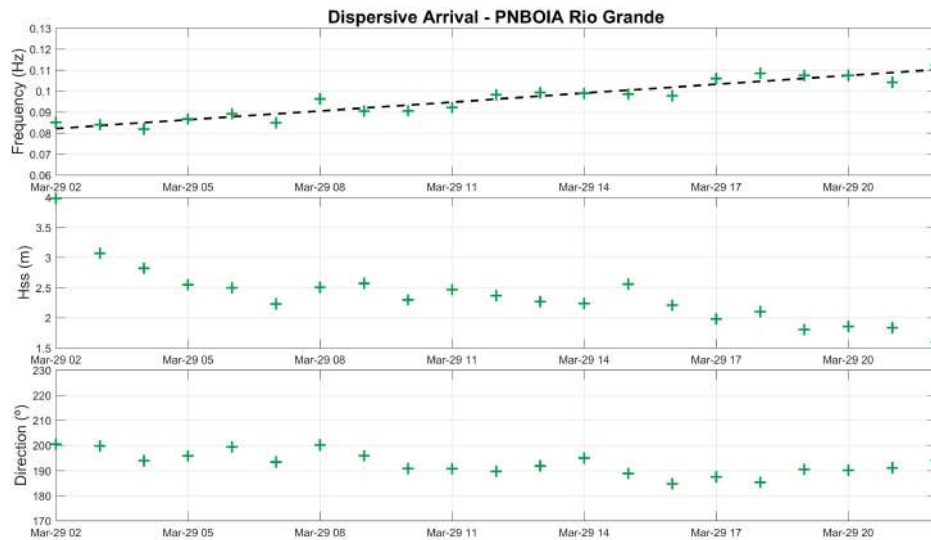

Figure A.17: Dispersive arrival event recorded at buoy RG on March 2012.
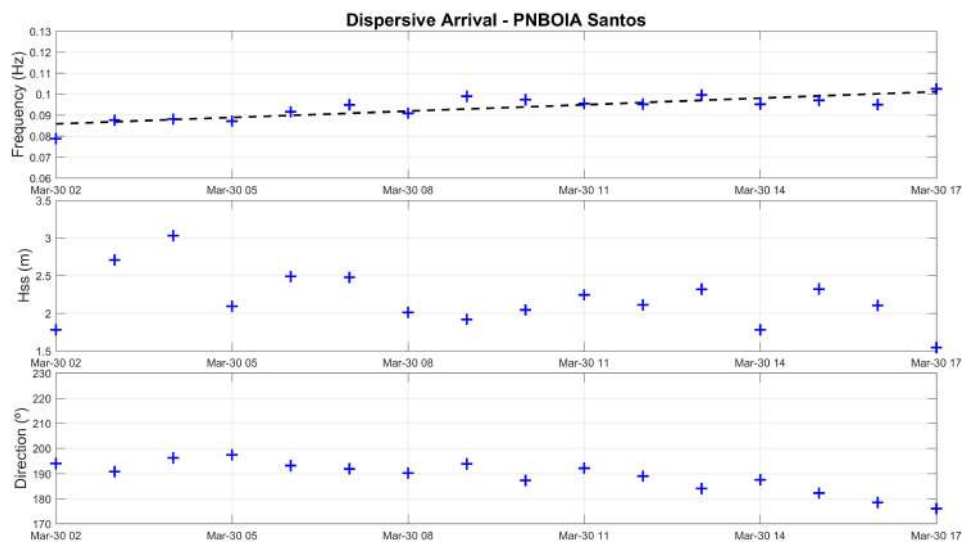

Figure A.18: Dispersive arrival event recorded at buoy SA on March 2012.

As shown on table A.4, the storm possible responsible for the swell generation is

located at least 2000 km far from buoy RG site. Figure A.19 shows cyclogenesis area on CFSR wind field at the times indicated by the fitting of dispersive arrivals (figures A.17 and A.18) as the moment of swell generation. Figure A.20 displays the relative vorticity field for March 26, 2012 at 13:00 UTC. From both, the wind pattern at 10 m height and the vorticity field, there is a clear indication of a huge cyclone (mean size of the order of 556 km) over the oceanic region offshore from South America. This cyclone seems to move at low speed (around 7.6 m/s) and after some time it moves towards the middle of the South Atlantic Ocean (not shown), not transferring more energy to swells after they leave the generation area.

Table A.4: Dispersive arrival recorded on March 2012. Distance, date and position of the storm estimated using the data fitting procedure, for both buoys RG and SA.

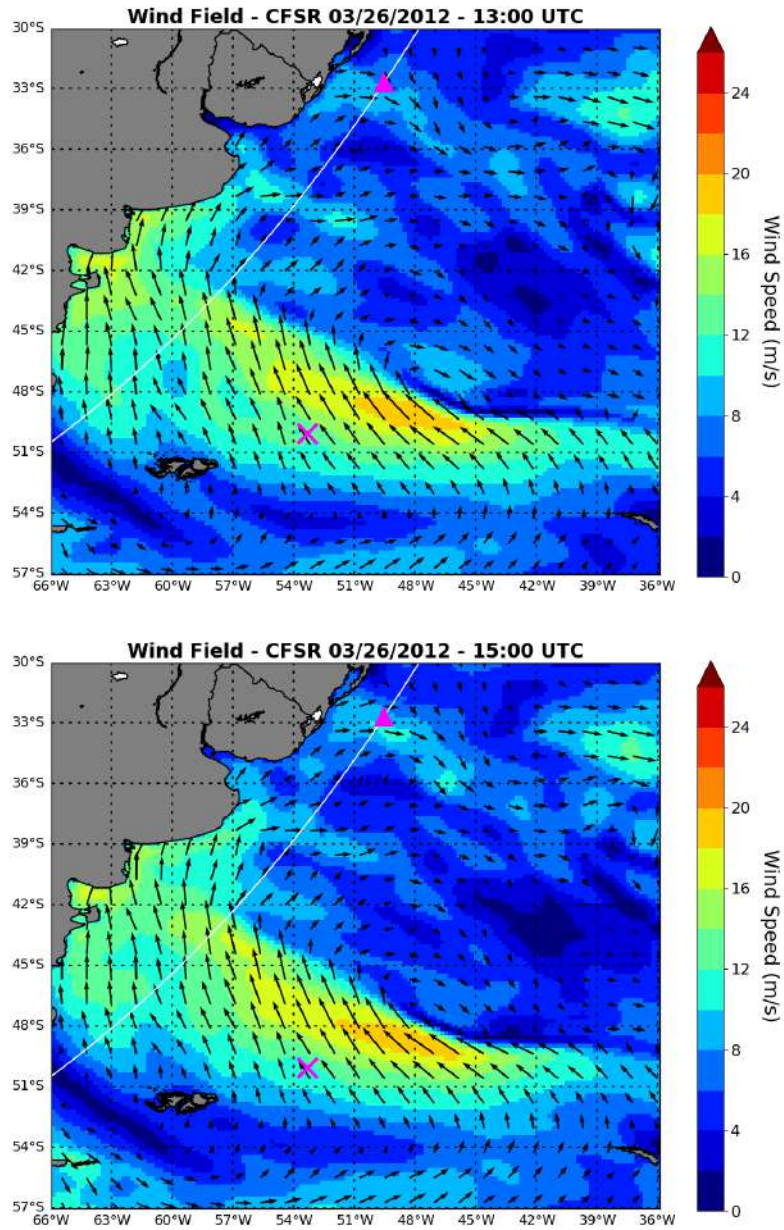|	**Buoy RG**	**Buoy SA**
Distance from storm	2007 km	2769 km
Date of the storm	03/26/2012 15 UTC	03/26/2012 13 UTC
Storm's position	-50.17°S / -55.71°W	-49.92°S / -50.92°W

Figure A.19: Wind field from CFSR referring to March 26, 2012 at 13 (top panel) and 15 (bottom panel) utc. The wind speed is represented by the colours while the direction is represented by the arrows. The white line shows the trajectory of the great circle that passes through the buoys RG and SA. The pink triangle indicates the buoy RG position and the pink x indicates the average swell source region obtained by dispersive arrival curves from RG and SA buoys.
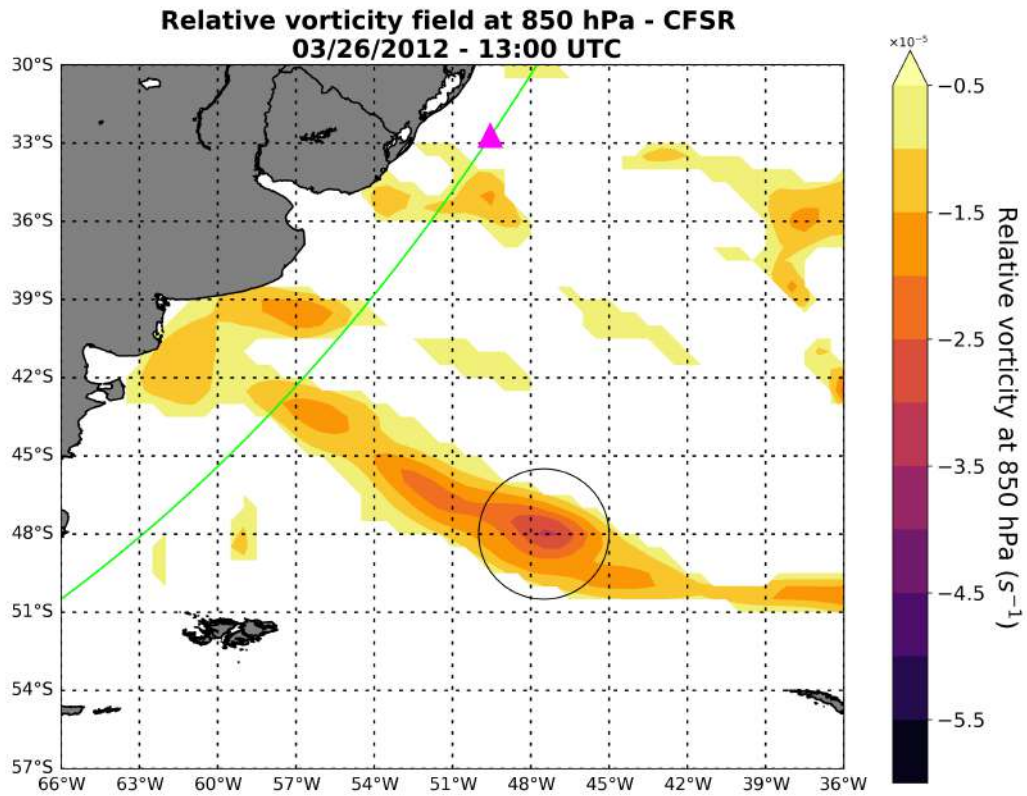
Figure A.20: Vorticity field estimated using wind field at 850 hPa from CFSR on March 26, 2012 at 13:00 UTC. The relative vorticity is represented by the colorbar. The green line depicts the great circle that passes at the buoys positions. The pink triangle indicates the position of buoy RG and the black circle indicates the average storm radius estimated using the local maximum of the vorticity field.